ACS Sustainable Chemistry & Engineering

Research Article

pubs.acs.org/journal/ascecg

Topological Analysis of Void Spaces in Tungstate Frameworks: Assessing Storage Properties for the Environmentally Important Guest Molecules and Ions: CO_2, UO_2, PuO_2, U, Pu, Sr^{2+}, Cs^+, CH_4, and H_2

Jacqueline M. Cole,*[,†,‡,§] Alisha J. Cramer,[†] and Anita Zeidler[§]

[†]Cavendish Laboratory, Department of Physics, University of Cambridge, J. J. Thomson Avenue, Cambridge CB3 0HE, United Kingdom

[‡]Argonne National Laboratory, 9700 S Cass Avenue, Argonne, Illinois 60439, United States

[§]Department of Chemistry, University of Cambridge, Lensfield Road, Cambridge CB2 1EW, United Kingdom

Supporting Information

ABSTRACT: The identification of inorganic materials, which are able to encapsulate environmentally important small molecules or ions via host−guest interactions, is crucial for the design and development of next-generation energy sources and for storing environmental waste. Especially sought after are molecular sponges with the ability to incorporate CO_2, gas pollutants, or nuclear waste materials such as UO_2 and PuO_2 oxides or U, Pu, Sr^{2+}, or Cs^+ ions. Porous framework structures promise very attractive prospects for applications in environmental technologies, if they are able to incorporate CH_4 for biogas energy applications or to store H_2, which is important for fuel cells, e.g., in the automotive industry. All of these applications should benefit from the host being resistant to extreme conditions such as heat, nuclear radiation, rapid gas expansion, or wear and tear from heavy gas cycling. As inorganic tungstates are well known for their thermal stability and their rigid open-framework networks, the potential of $Na_2O-Al_2O_3-WO_3$ and Na_2O-WO_3 phases for such applications was evaluated. To this end, all known experimentally determined crystal structures with the stoichiometric formula $M_aM'_bW_cO_d$ (M = any element) are surveyed together with all corresponding theoretically calculated $Na_aAl_bW_cO_d$ and $Na_xW_yO_z$ structures that are statistically likely to form. Network descriptors that categorize these host structures are used to reveal topological patterns in the hosts, including the nature of porous cages, which are able to accommodate a certain type of guest; this leads to the classification of preferential structure types for a given environmental storage application. Crystal structures of two new tungstates $NaAlW_2O_8$ (**1**) and $NaAlW_3O_{11}$ (**2**) and one updated structure determination of $Na_2W_2O_7$ (**3**) are also presented from in-house X-ray diffraction studies, and their potential merits for environmental applications are assessed against those of this larger data-sourced survey. Overall, results show that tungstate structures with three-nodal topologies are most frequently able to accommodate CH_4 or H_2, while CO_2 appears to be captured by a wide range of nodal structure types. The computationally generated host structures appear systematically smaller than the experimentally determined structures. For the structures of **1** and **2**, potential applications in nuclear waste storage seem feasible.

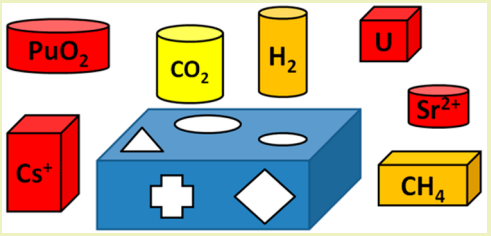

KEYWORDS: *Host−guest, Tungstate, Framework structure, Energy fuel storage, CO_2 emissions, Nuclear waste storage*

INTRODUCTION

For many years, porous materials have garnered considerable attention, owing to the wide range of applications that they potentially offer. The removal of pollutants from industrial waste,[1−3] the selective removal and storage of radioactive ions from nuclear waste,[4−7] and the storage of small molecules in alternative energy technologies[8−10] illustrate just a few of many possibilities. Currently, the focus of interest seems to be centered on organic−inorganic hybrid materials, generally known as metal−organic frameworks (MOFs), as these can be custom-tailored to a specific pore size.[3,8,11−17] Thus, MOFs have already demonstrated their potential as storage materials for alternative fuels such as CH_4 and H_2,[8,15,17−19] as CO_2 reservoirs for pollution-control measures,[3,20] or more recently for the potential uptake of volatile organic compounds.[21,22] The high level of success that MOFs have enjoyed sparked a search for other types of molecular architectures, which could be employed for similar tasks; this has led to the development of organic analogues of MOFs, of the so-called covalent organic frameworks (COFs).[23] Like MOFs, COFs have already proven their potential as storage materials for H_2, CH_4, CO_2, and N_2.[9,10] However, for applications involving harsher environmental pollutants, such as the storage of radioactive waste or

Received: April 29, 2015
Revised: July 14, 2015
Published: July 15, 2015

DOI: 10.1021/acssuschemeng.5b00369
ACS Sustainable Chem. Eng. 2015, 3, 2112−2129

volatile organic compounds, purely inorganic materials continue to dominate in practice.[1,2,4−7,24,25]

In order to determine the suitability of potential candidates for these types of applications, the void spaces in their crystalline solid-state frameworks should be examined initially. After all, only if the guest molecule can be accommodated in the host are further considerations appropriate. In the ongoing search for usable materials, data mining of structure databases can provide a useful tool to identify potential candidates for the applications in hand. For example, a study on Li^+ migration maps[26] examined the structure of channels within lithium-containing inorganic compounds using Voronoi−Dirichlet partitioning that is implemented in the crystallographic topological analysis program TOPOS.[27] That study identified 277 out of 2171 crystal structures which contained suitable conduction channels; 26 of these structures, despite not being previously known as solid electrolytes, showed potential promise as ionic conductors.

We herein propose to employ Voronoi−Dirichlet partitioning to investigate the void space within cages of three-dimensional tungstate-based extended framework structures in a similar way, i.e., by using topological net descriptors for comparisons in order to conduct a void-space analysis for identifying possible host/guest combinations. To the best of our knowledge, this represents the first topological analysis of a large survey of tungstate structures, which are sourced from experimental and computational data. Experimental data emanate from the Inorganic Crystal Structure Database (ICSD) and from in-house crystallographic studies of three phases of Na_2O-WO_3. Computational data were obtained from a structure prediction approach, determining all structures containing Na^+, W^{6+}, and O^{2-} ions with or without Al^{3+} ions, which are statistically likely to form based on ionic substitution considerations of known related structures. The topological nets and void volumes of all these crystal structures are determined and compared in order to assess their potential as hosts in host/guest media with environmental applications.

In the context of nuclear waste storage applications, the UO_2 and PuO_2 oxides, U and Pu ions of various oxidation states, and Sr^{2+} and Cs^+ ions are explored as possible guests, out of the myriad of waste products found in nuclear waste. Waste from nuclear facilities, in the form of spent nuclear fuel, is found predominantly in the form of uranium or plutonium oxides.[28] Furthermore, current efforts, especially among tungstates, are largely focused on encapsulating radioactive waste via ion-exchange,[4−7,24,29] making the containment of U and Pu ions also important. Meanwhile, high activity fission product radionuclides Cs^+ and Sr^{2+} provide an additional focus for storage development. Within waste streams from nuclear reactors, ^{137}Cs and ^{90}Sr generate most of the thermal heat found in high level waste, and combined with their relatively short half-lives (<50 years), processing these two elements separately from the rest of the waste stream is both practical and beneficial.[30] In the context of environmental waste associated with climate change, the encapsulation of CO_2 is evaluated with a view to offset carbon emissions. Meanwhile, the possible inclusion of CH_4 and H_2 molecules is considered for alternative energy storage applications, which stand to deter carbon emissions.

The diverse origins of the obtained data also provide the opportunity to make a general comparison of experimentally determined against theoretically calculated structures for this family of inorganic materials and to establish a relative ranking of the likely use of three in-house characterized subject materials $Na_aAl_bW_cO_d$ (a = 1,2; b = 0,1; c = 2,3; d = 7,8,11) within this representative set of all statistically conceivable tungstate framework structures.

The overarching workflow associated with this topologically generated data-mining study that pairwise matches host−guest volumes is illustrated in Figure 1.

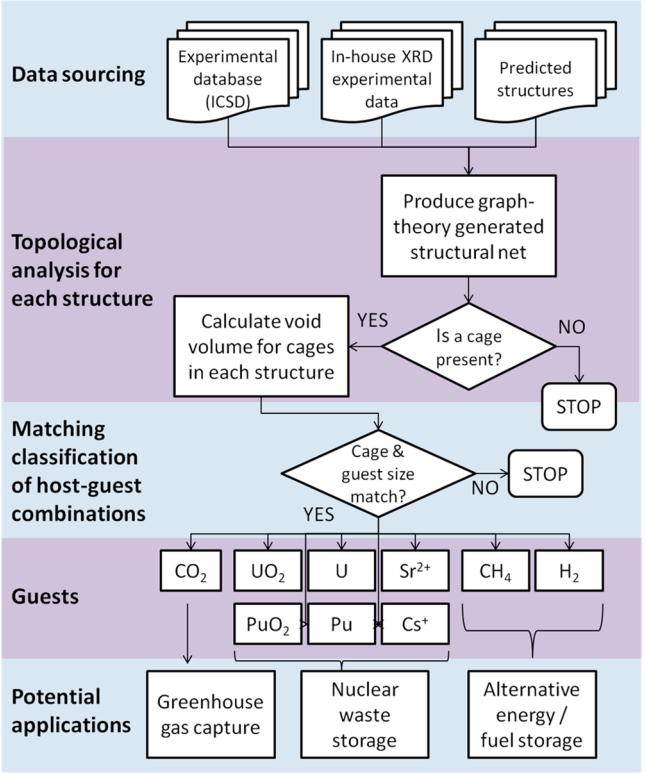

Figure 1. Overarching workflow for suiting host−guest pairs in tungstate-based structures with porous cages for guest inclusion.

EXPERIMENTAL AND COMPUTATIONAL METHODS

Experimentally Derived Crystal Structure Data of Tungstate Framework Structures. Data for all 378 previously reported crystal structures of ternary and quaternary tungstates of the general formulae $M_aW_yO_z$ or $M1_aM2_bW_yO_z$ (M, M1, M2 = any metal) were extracted from the Inorganic Crystal Structure Database (ICSD); 284 of this total, which displayed structural frameworks that produce cages, were taken forward for full data analysis. Search parameter filters within the ICSD restricted structures to those containing W, O, and either three or four total element species. From the results, disordered structures and those with partial occupancy in one or more of the atomic sites were manually excluded. The remaining list of structures was further refined by manually removing duplicates (structures with the same chemical formula and spacegroup); among duplicate structures, those with the lowest R1 factor were kept.

In-House Provision of Crystal Structure Data: Sample Preparation and Characterization of Three Na_2O−Al_2O_3−WO_3 and Na_2O−WO_3 Phases. Samples were prepared as previously described elsewhere.[31] The crystal structures of two new compounds $NaAlW_2O_8$ (**1**) and $NaAlW_3O_{11}$ (**2**) were determined by single crystal X-ray diffraction. Furthermore, the crystal structure of $Na_2W_2O_7$ (**3**) was determined at low temperature (T = 180(2) K), affording an improved structural model on the previously reported room-temperature structure.[32]

DOI: 10.1021/acssuschemeng.5b00369
ACS Sustainable Chem. Eng. 2015, 3, 2112−2129

Suitable single crystals were mounted onto glass fibers using perfluoropolyether oil. Diffraction data for (**1**) were collected on a Nonius Kappa CCD diffractometer, equipped with a monochromatic Mo Kα (λ = 0.71073 Å) X-ray source and an Oxford Cryosystems Cryostream open-flow N_2 cooling device. Cell parameters were refined against data from all regions of reciprocal space using HKLScalepack.[33] Data reduction employed HKLDenzo and Scalepack,[33] while data sets were corrected for Lorentz and polarization effects, as well as for absorption using SORTAV.[34] Diffraction data for (**2**) and (**3**) were collected on a Rigaku Saturn 724+ CCD diffractometer, equipped with a monochromatic Mo Kα (λ = 0.71073 Å) X-ray source, SHINE Optics, and an Oxford Cryosystems CryostreamPlus open-flow N_2 cooling device. Cell refinement, data collection, and data reduction were carried out with Rigaku CrystalClear-SM Expert 2.0 software,[35] whereas absorption correction was implemented using ABSCOR.[36]

All structures were solved with direct methods and refined by full-matrix least-squares methods on F2 using SHELXL-97.[37] Full details for crystal, data collection, and refinement parameters are provided in the Supporting Information.

A few specific technical notes about the structure solution and refinement of (**1**)−(**3**) are worth mentioning. Owing to its pseudo-orthorhombic unit cell, the structure of (**1**) displays a small, but nevertheless distinct, pseudomerohedral twin component, resulting in a fractional twin contribution of 0.16(3)%. Compound (**2**) displays significant structural disorder, to the extent that its elemental and stoichiometric composition needed verification from energy-dispersive X-ray (EDX) analysis to aid crystal structure determination. The EDX experiment employed a Zeiss Cross Beam scanning electron microscope, which afforded the following elemental proportions: Na = 5.47%; Al = 5.13%; W = 15.54%; O = 65.62%. A residual 8.34% arising from a contribution of carbon was attributed to surface contamination. These results were particularly important in checking that the compound contained Al, rather than Cr, which could have substituted Al as a reaction contaminant. The structure of (**3**) matches the previously determined crystal structure of this material,[32] albeit with improved refinement statistics and different thermal parameters owing to the low-temperature data collection nature of this new study.

Theoretically Calculated Predictions for Tungstate Structures. All hypothetically possible crystal structures containing any statistically conceivable combination of W, P, Al, and O ions were generated computationally by using previously described methods.[38] The possibility of individual crystal structures was based on the statistical probability for existing structural motifs in the Inorganic Crystal Structure Database (ICSD) to be transmuted into tungstates via ionic substitution. The probability of ionic substitution was determined via a reference pair correlation matrix of various ion combinations, where each matrix element, g_{AB}, represents the probability of ionic substitution between a given pair of ions A and B. This probability has been precalculated by enumerating the relative number of crystal structure examples in the ICSD, which differ only in the ions A and B. This method accordingly assesses the relative ease by which a given ion can fit into the crystallographically equivalent site of another ion. Values for g_{AB} were therefore derived from a pretrained reference library of structural homologues of A and B. While this was not part of the probabilistic calculation, it is hardly surprising that two ions of similar size, chemical properties (e.g., from the same group in the periodic table), and/or identical charge tend to have higher g_{AB} values since substitution for each proceeds more readily. For example, when A = W^{6+}, the highest g_{AB} value was obtained for B = Mo^{6+}, whereas when A = Al^{3+}, large g_{AB} values were obtained for B = Cr^{3+}, Fe^{3+}, In^{3+}, or Ga^{3+}.

Only charge-balanced crystal structures, and those not already in the ICSD, were considered in the theoretical structure prediction results. In total, 196 hypothetical tungstate structures of the general formula $Na_mW_nAl_oO_p$ were generated computationally; 43 of these calculated structures were taken forward for full void-space analysis since only these produced cages, which are of course necessary for hosting guest molecules or ions.

Topological Analysis. *TOPOS Methods.* All selected tungstate structures were assessed for their potential for hosting the subject guest molecules and ions, using the crystallographic topological analysis program package, TOPOS 4.0 Professional.[27] This enabled the topological classification of each tungstate structure, and the determination and analysis of the void space residing within its framework.

This analysis was accomplished by first defining the topological net of each structure using the ADS module in TOPOS. Such nets were identified using graph theory to calculate a map of the circuits contained therein by viewing all atoms as nodes, and all bonds as edges, thereby ascertaining the geometrical patterns in the crystal structure. These nets were then categorized as n-nodal in the presence of *n* different kinds of inequivalent vertices in the net. The net may contain tiles, defined as generalized polyhedra (cages), which have at least two edges incident upon each vertex and two faces incident upon each edge.[39,40] These tiles are described according to how many faces a given tile possesses with each face being defined by its m-membered rings. This nodal/tiling topological representation is illustrated in Figure 2, using the example of (**1**). The full classification of a net is

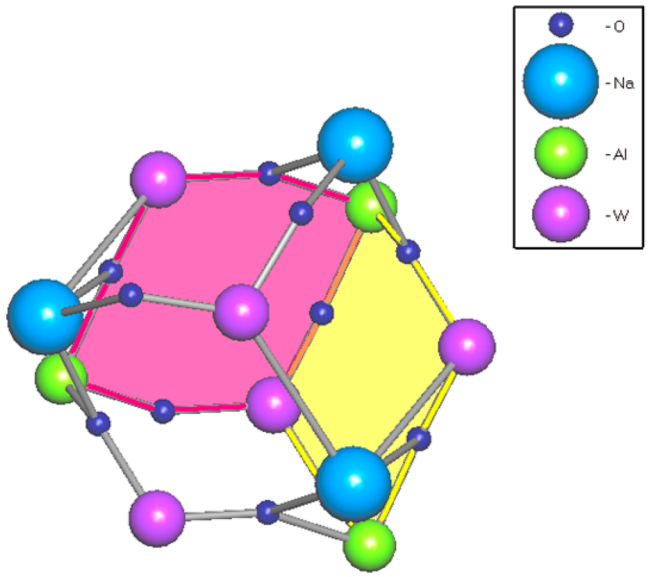

Figure 2. A 22/11 cage using (**1**) as the example: $[3^2.4^3.6.7^2.8^3]$ tile, whereby 22/11 denominates the total number of nodes/faces; $[3^2.4^3.6.7^2.8^3]$ indicates the presence of two faces consisting of three-membered rings, three faces consisting of four-membered rings, one face consisting of six-membered rings, two faces consisting of seven-membered rings (e.g., yellow plane), and three faces consisting of eight-membered rings (e.g., pink plane).

based on several conventional descriptors, which may be used to search the TOPOS Topological Database (TTD) for the topological type of the net (for a full explanation and list of these descriptors see[41,42]).

Void-space analysis was then accomplished via a two-step process. The first step is the determination of all cages found within each structure, prior to calculating the void-space volume within each cage using Voronoi−Dirichlet polyhedra (VDP). Thus, a comparison basis for the cavity volumes in each structure was established in the first step. Cages can be found from the net topology and were determined using the ADS module in TOPOS. For three-dimensional periodic framework structures, the circuits formed by the atoms and bonds can be combined to form generalized polyhedra that are topologically equivalent to spheres. For an in-depth discussion of cages and tiling, see refs 39 and 43.

The second step of void-space analysis comprises the calculation of a Voronoi−Dirichlet partition of the crystal space for each cage, using the Dirichlet module in TOPOS to construct the VDP for all independent framework atoms. From this partition, the location and size of voids were obtained by placing a node at the intersection of

DOI: 10.1021/acssuschemeng.5b00369
ACS Sustainable Chem. Eng. 2015, 3, 2112−2129

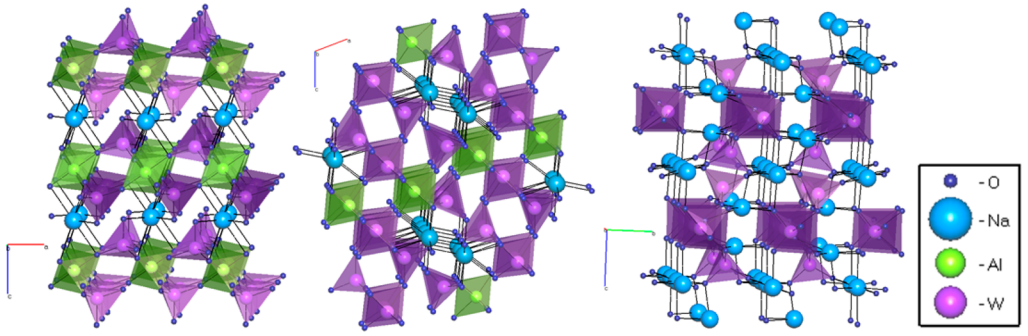

Figure 3. Crystal structures of (**1**) and (**2**) viewed down the *b*-axis (left and middle) and (**3**) viewed down the *a*-axis (right).

four or more VDP vertices. Subsequently, the Voroni−Dirichlet partition was reconstructed taking the void nodes into account, which resulted in a map of the void space of the structure. In order to analyze the cavity size within individual cages, the cages were isolated and void nodes were generated from the atoms forming the cage. Subsequently, VDP were generated for these void nodes, from which their volumes were calculated.

Guest Volume Determination. The intrinsic volumes of the guest molecules or ions were estimated in three different ways. For individual atoms or ions, U, Pu, Cs^+ and Sr^{2+}, radii of 1.75, 1.75, 2.60, and 2.00 Å, respectively, were obtained from the Slater radii[44] database in TOPOS. Subsequently, these radii where employed to calculate spherical volumes. The volumes of the UO_2 and PuO_2 oxides were extracted from their previously reported experimentally determined crystal structures, as sourced from the ICSD. Owing to the three-dimensional frameworks formed by UO_2 and PuO_2 crystal structures, volume determination of discrete molecules was unfeasible. Hence, the volumes of a single U or Pu, and the eight valence-bonded oxygens for each, were determined for chosen samples of UO_2[45] and PuO_2,[46] respectively.

Volumes for small guest molecules, such as CO_2, CH_4, and H_2, were established based on previously published kinetic diameters (3.3, 3.8, and 2.89 Å, respectively), from which spherical volumes were calculated. As the kinetic diameter represents only the smallest dimension of a given molecule, the calculated spherical volumes are necessarily the smallest possible volume for that molecule, and there is no consideration of the shape of the molecule in this calculation. This is acceptable as long as an upper bound of guest volumes within a cage can be set to provide the necessary latitude to allow for the molecule size to be greater in its other dimensions.

The resulting volumes for all guest molecules and ions were rounded up to the nearest whole integer in order to establish the lowest bound of the desired cage size. An upper bound was set 4 $Å^3$ above this lower bound, which should allow the guest some spatial flexibility, without allowing more than one guest within a single cage. An exception to this is H_2, where a maximum of two molecules may fit in a cage at the upper limit.

RESULTS AND DISCUSSION

New Crystal Structures. *$NaAlW_2O_8$ (1).* The W−Al network in (**1**) consists of four-membered rings with alternating octahedrally coordinated Al and tetrahedrally coordinated W ions, whereby Na ions occupy the space between rings (Figure 3, left). One might naturally suppose that the framework of (**1**) would be isostructural to the previously reported $MM'W_2O_8$ (M, M′ = metal) crystal structures, $NaCrW_2O_8$ and $NaInW_2O_8$, which form layers of polyhedra in the order Na, W, In/Cr, W, Na yielding a 2-nodal net of the α-PbO_2 topological type.[47] However, it is not; instead, (**1**) turns out to be isomorphic with the molybdate compound, $NaAlMo_2O_8$,[48] manifesting coordination polyhedra that form a 6-nodal topological net.

All atoms in the structural framework of (**1**) lie on general positions with the exception of the Al, which is located on an inversion center. The observed W···O bond lengths range from 1.743(5)−1.806(4) Å, whereas the Al···O bond lengths range from 1.874(4)−1.891(4) Å, and the Na···O bond lengths span a range from 2.367(4)−2.924(4) Å.

$NaAlW_3O_{11}$ (2). Compound (**2**) features two tetrahedrally and one octahedrally coordinated W, as well as one octahedrally coordinated Al, forming the main part of the network, with Na ions occupying sites inside the framework. The W−Al network adopts a 2-nodal net which corresponds to a standard toplogical type, 3,6T36. This network consists of four-membered rings of alternating octahedrally coordinated W and Al, which are connected via their apexes to four-membered rings of alternating octahedrally coordinated Al and tetrahedrally coordinated W ions (Figure 3, middle). Inclusion of the Na ions results in the formation of a 9-nodal net.

$Na_2W_2O_7$ (3). In contrast to (**1**) and (**2**), (**3**) lacks any Al ions, and so the coordination sites of its structure contain exclusively octa- and tetrahedrally coordinated W ions (Figure 3, right). Topologically, this can be classified as a 9-nodal net. The W network contains long chains of octahedrally coordinated W, wherein the tetrahedrally coordinated W ions adopt alternating positions on both sides of the chain. The Na ions occupy coordination sites between these chains, coordinating to the terminal oxygens of the tetra- and octahedrally coordinated W ions.

Guest−Host Comparisons for Environmental Applications. In total, 577 crystal structures of tungstate-based extended frameworks were surveyed for their prospects as host materials for the environmentally important guest molecules or ions: CO_2, UO_2, PuO_2, U, Pu, Sr^{2+}, Cs^+, CH_4, and H_2. Of this total, 196 were hypothetical crystal structures generated from computational predictions, while the other 381 were sourced from (378) previously reported or (3) in-house data from diffraction experiments. Of these, 284 previously reported crystal structures, 43 hypothetical structures, and the 3 in-house determined structures produced topological tilings; the 10 largest cages in these 330 tilings were subsequently identified, and their corresponding void volumes calculated (Supporting Information). Possible guest−host matches were then assessed by comparing these void-space volumes of the framework structures against the size of each subject guest molecule or ion.

CO_2 Capture. The optimal cavity size for the incorporation of CO_2 was determined using its kinetic diameter of 3.3 Å,[49] providing a target volume of 19−23 $Å^3$. The structural analysis identified 52 previously reported experimentally determined crystal structures containing 60 cages with appropriate void-space volumes. Of these, 47 structures had one suitable cage

DOI: 10.1021/acssuschemeng.5b00369
ACS Sustainable Chem. Eng. 2015, 3, 2112−2129

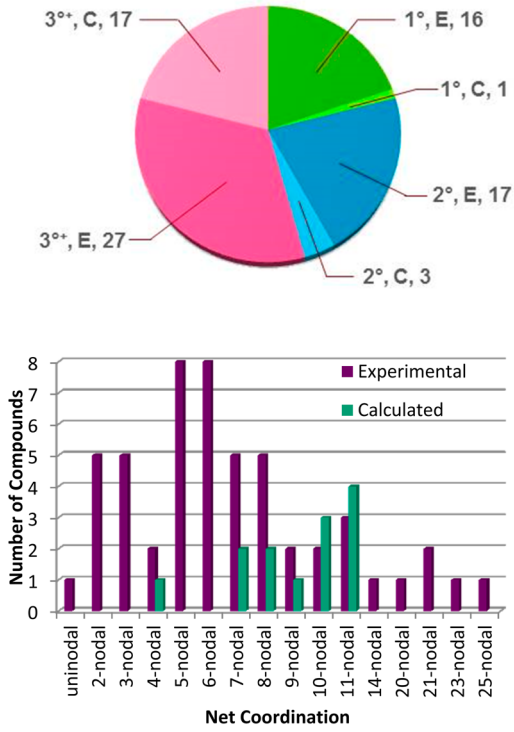

Compound	Cage attribute	Ref. [ICSD -paper]
$Li(NbWO_6)$	E, 1°	45799 – [50]
$Li(TaWO_6)$	E, 1°	45800 – [50]
$Na(NbWO_6)$	E, 1°	45802 – [50]
$Na(TaWO_6)$	E, 1°	45803 – [50]
$Na(VWO_6)$	E, 1°	174133 – [51]
$BiNdWO_6$	E, 1°	416789 - [52]
$KEu(WO_4)_2$	E, 1°	173634 - [53]
Ba_2SrWO_6	E, 1°	246115 - [54]
$Gd_3(BWO_9)$	E, 1°	250417 - [55]
$Nd_3(BWO_9)$	E, 1°	250415 - [55]
$Sm_3(BWO_9)$	E, 1°	250416 - [55]
$Pr_3(BWO_9)$	E, 1°	250414 - [55]
$Ba_{11}(W_4O_{23})$	E, 1°	418207 - [56]
$Li_2Zn_2(W_2O_9)$	E, 1°	160509 - [57]
$La_2(WO_4)(Te_3O_7)_2$	E, 1°	249538 - [58]
Ba_2SrWO_6	E, 1°- 3°	246108 - [54]
$Gd(WO_4)Cl$	E, 2°	35292 - [59]
Ba_2SrWO_6	E, 2°	246113 - [54]
$Eu_2(MoW_2O_{12})$	E, 2°	155946 - [60]
$Na_4Th(WO_4)_4$	E, 2°	422185 - [61]
$Na_5Lu(WO_4)_4$	E, 2°	200930 - [62]
$Na_5Tb(WO_4)_4$	E, 2°	20426 - [63]
$Na_5La(WO_4)_4$	E, 2°	20427 - [63]
$Sr_8Cu(WO_6)_3$	E, 2°	183646 - [64]
$Hg(WO_4)$	E, 2°	169670 - [65]
$K(W_3O_9)$	E, 2°	100228 - [66]
$K_2W_4O_{13}$	E, 2°	2412 - [67]
$Eu_2(Mo_2WO_{12})$	E, 2°	155945 - [60]
$Hg_2(WO_4)$	E, 2°	90085 - [68]
Ba_2WO_5	E, 2°	62489 - [69]
$K_2(WO_4)$	E, 2°	150840 - [70]
$Li_2(W_2O_7)$	E, 2°- 3°	1897 - [71]
$ErBi(W_2O_9)$	E, 3°	183443 - [72]
$EuBi(W_2O_9)$	E, 3°	183444 - [72]
$SmBi(W_2O_9)$	E, 3°	183445 - [72]
$Na_3F(WO_4)$	E, 3°	417289 - [73]
$Na_5Y(WO_4)_4$	E, 3°	417143 - [74]
UW_2O_{11}	E, 3°	81983 - [75]
Cu_2WO_4	E, 3°	62058 - [76]
$Pb_3(WO_5)Cl_2$	E, 3°	89833 - [77]
$CuDy(WO_4)_2$	E, 4°	73749 - [78]
$CuEr(WO_4)_2$	E, 4°	73747 - [78]
$CuLa(W_2O_8)$	E, 4°	68614 - [79]
$Tl_2(WO_4)$	E, 4°	8212 - [80]
$Ce_{10}W_{22}O_{81}$	E, 4°- 5°	260095 - [81]
$Cu_2(WO_4)$	E, 5°	202669 - [82]
$FeCe(WO_4)(W_2O_8)$	E, 6°	401919 - [83]
$K_2Nb_{10}W_7O_{47}$	E, 6°	62130 - [84]
$Al_2(WO_4)_3$	E, 6°	73878 - [85]
$Al_2(WO_4)_3$	E, 6°	90936 - [86]
$Ag_{26}I_{18}(WO_4)_4$	E, 6°- 9°	56852 - [87]
$Al_2(WO_4)_3$	E, 9°- 10°	56827 - [85]
$Na_2W_2O_7$	C, 1°	
Na_2WO_4	C, 2°	
Na_2WO_4	C, 2°- 4°	
$Na_2W_2O_7$	C, 2°- 4°	
$Na_2W_2O_7$	C, 3°	
$Na_2W_2O_7$	C, 3°- 4°	
Na_2WO_4	C, 4°	
$Na_2W_2O_7$	C, 4°	
$NaAlW_2O_8$	C, 4°	
$NaAlW_2O_8$	C, 4°	
$NaAlW_2O_8$	C, 4°- 5°	
$Na_2Al_2WO_7$	C, 4°- 5°	
$Na_2W_2O_7$	C, 7°- 8°	

Figure 4. (Left) Distribution of cage types (1°, 2°, 3°+) of host structures comprising n-nodal nets that can incorporate CO_2, according to their frequency observed in experimental (E) and calculated (C) crystal structures. (Right) List of their associated compound identifiers (ICSD number and ref citation).

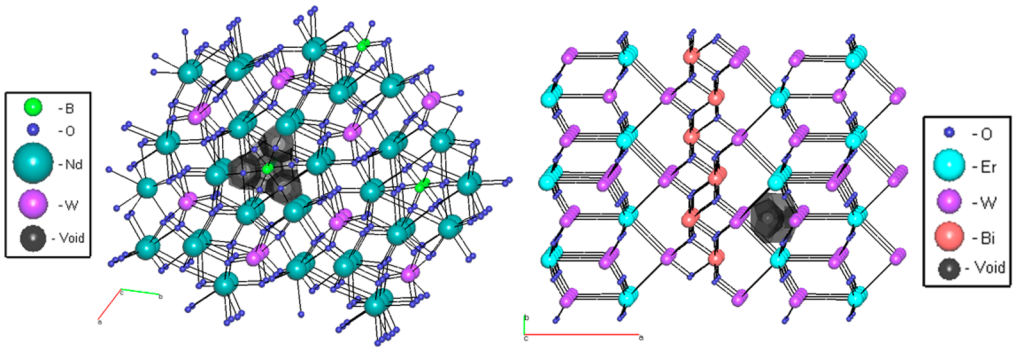

Figure 5. Representative example host framework structures from the two most common types of n-nodal nets whose cages have suitable void-space volumes (black/gray) to accommodate CO_2 molecules: 5-nodal (left; $Nd_3(BWO_9)$ [ICSD ref 250415[55]]) and 6-nodal (right; $ErBi(W_2O_9)$ [ICSD ref 183443[72]]).

volume per structure; the remaining 5 structures contained two or more suitable cages (hereafter designated as "multiple cages") per structure. The subsequent breakdown of all suitable cages by type found that 16 cages suited for hosting a guest were found to be the largest (primary, 1°) cage formed by the structure, whereas in 17 of the cages it was the secondary (2°) cage with suitable void space, and 27 cages of interest were tertiary (3°) or higher (3°+). Furthermore, five of the compounds contained at least two cages suitable for CO_2 storage. Among the calculated structures, a total of 13

DOI: 10.1021/acssuschemeng.5b00369
ACS Sustainable Chem. Eng. 2015, 3, 2112–2129

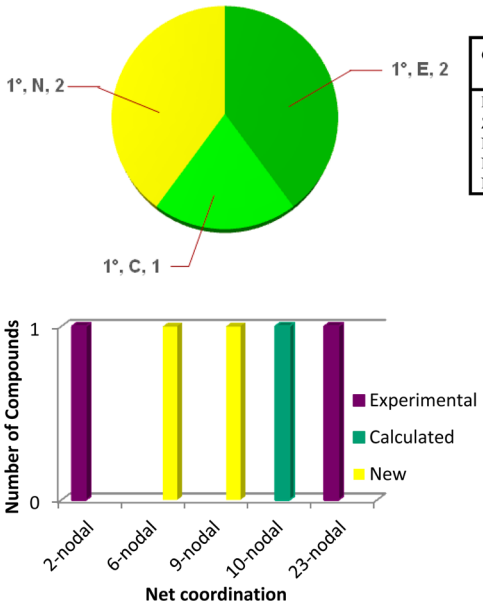

Compound	Cage attribute	Ref. [ICSD - paper]
$FeCe(WO_4)(W_2O_8)$	E, 1°	401919 - [83]
$Zr(WO_4)_2$	E, 1°	262062 - [88]
$NaAlW_2O_8$	N, 1°	This work – [(1)]
$NaAlW_3O_{11}$	N, 1°	This work – [(2)]
$Na_2W_2O_7$	C, 1°	

Figure 6. (Left) Distribution of cage types (1°) of host structures comprising n-nodal nets that can incorporate UO_2, according to their frequency observed in previously reported (E) or newly determined (N) experimental and calculated (C) crystal structures. (Right) List of their associated compound identifiers (ICSD number and ref citation).

structures were found to contain 21 suitable cages (1 × 1°; 3 × 2°; 17 × 3°$^+$), with seven of the structures exhibiting multiple cages. None of the in-house experimentally determined crystal structures ((**1**)−(**3**)) were found to contain cages suitable for CO_2 containment. Figure 4 summarizes these statistics, while representative example structures from the most common (5- and 6-nodal) nets that demonstrate capacity to host CO_2 are displayed in Figure 5.

Nuclear Waste Storage. *UO_2.* The potential inclusion of UO_2 was examined on the basis of the TOPOS-generated VDP volume for a single cube of eight-coordinated U from the UO_2 crystal structure (ICSD ref 246851[45]; space group $Fm\bar{3}m$; unit cell a = 5.468 Å). This produced a void-space volume of 63.09 Å^3, which gave a targeted void-space volume of 64−68 Å^3. This range identified only two suitable cages within previously reported structures, one within predicted structures and two within the in-house structures ((**1**) and (**2**)), as shown in Figure 6. All structures contained only 1° cages. With such a limited sampling, there is no net type that is more common than any other for hosting UO_2. As such, (**1**) will serve as the representative example structure with a 6-nodal net, shown in Figure 7.

PuO_2. Determination of the PuO_2 volume followed the same general pattern as for UO_2. The VDP volume of a single cube of eight-coordinated Pu was obtained from TOPOS using the PuO_2 crystal structure (ICSD ref 55456[46], space group $Fm\bar{3}m$, unit cell a = 5.3982 Å). This afforded a target void-space volume range of 61−65 Å^3. The topological analysis identified eight suitable cages among seven previously reported crystal structures (6 × 1°; 2 × 2°), with one structure containing both 1° and 2° cages of a suitable size, a 3° cage in one predicted structure, and a 1° cage in the new structure, (**2**). Figure 8 summarizes these statistics. Figure 9 provides a representative example of a tungstate-based framework structure belonging to the most common type of n-nodal net (n = 9) that bears a cage suitable for PuO_2 containment.

U or Pu Ions. Although it would be more accurate to investigate ions, differences in reactor type, reprocessing, and

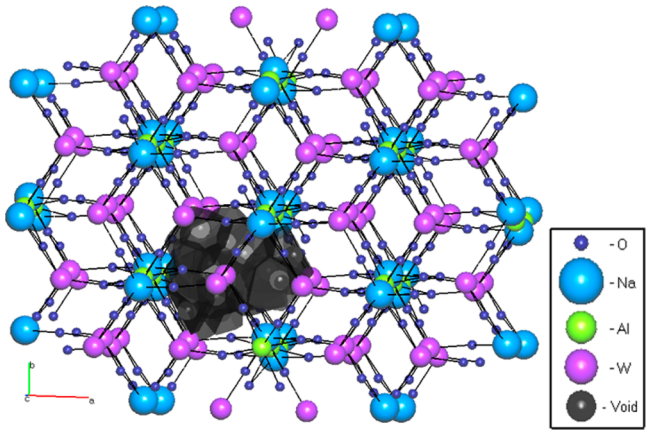

Figure 7. Representative example of a crystal structure (of $NaAlW_2O_8$ [this work (**1**)]) bearing a (n = 6) n-nodal net that contains cages with suitable void-space volumes (black/gray) to accommodate UO_2.

waste management techniques can result in different states of a given ion within the waste material. In natural water−rock systems, Pu has four oxidation states (3$^+$, 4$^+$, 5$^+$, 6$^+$), while U can often be found as U^{4+} or U^{6+};[94] as such, it was decided to use the atomic radii for these elements since this represents the largest volume that would potentially be necessary for encapsulation. U and Pu atoms presented the same Slater radii[44] listings in TOPOS and so were considered together in terms of finding suitable host structures to contain them. The associated target void-space volumes were 23−27 Å^3. This resulted in the selection of 45 previously reported crystal structures that feature 68 suitable cages (11 × 1°; 18 × 2°; 39 × 3°$^+$; 13 × multiple cages); 13 predicted structures (2 × 1°; 6 × 2°; 6 × 3°$^+$), one of which contains both a 2° and 3° cage; and one newly determined crystal structure ((**3**), bearing a 2° cage). Figure 10 displays these results. A representative example structure, bearing the most common type of n-nodal net (n = 3) whose cages appear to be able to host U or Pu ions, is presented in Figure 11.

DOI: 10.1021/acssuschemeng.5b00369
ACS Sustainable Chem. Eng. 2015, 3, 2112−2129

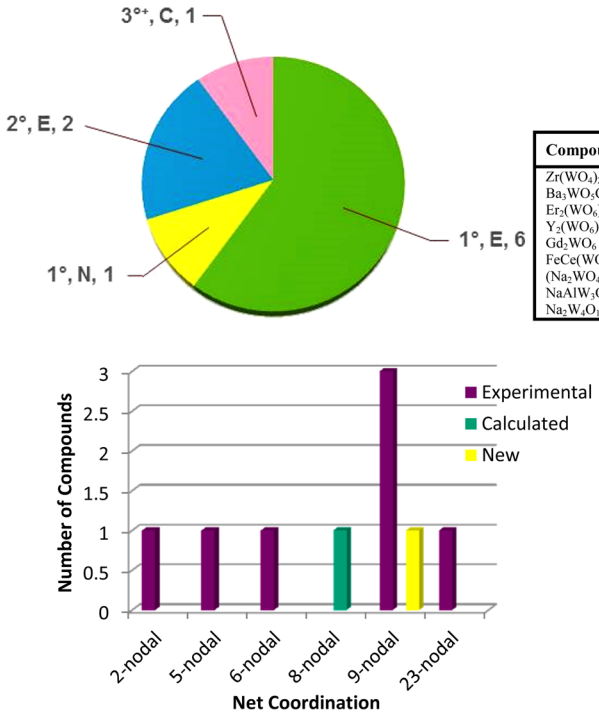

Compound	Cage attribute	Ref. [ICSD -paper]
$Zr(WO_4)_2$	E, 1°	262062 - [88]
$Ba_3WO_5Cl_2$	E, 1°	63518 - [89]
$Er_2(WO_6)$	E, 1°	62885 - [90]
$Y_2(WO_6)$	E, 1°	65811 - [91]
Gd_2WO_6	E, 1°	62888 - [92]
$FeCe(WO_4)(W_2O_8)$	E, 1° - 2°	401919 - [83]
$(Na_2WO_4)(H_2O)_2$	E, 2°	240882 - [93]
$NaAlW_3O_{11}$	N, 1°	This work – [(2)]
$Na_2W_4O_{13}$	C, 3°	

Figure 8. (Left) Distribution of cage types (1°, 2°, 3°) of host structures comprising n-nodal nets that can incorporate PuO_2, according to their frequency observed in previously reported (E) or newly determined (N) experimental and calculated (C) crystal structures. (Right) List of their associated compound identifiers (ICSD number and ref citation).

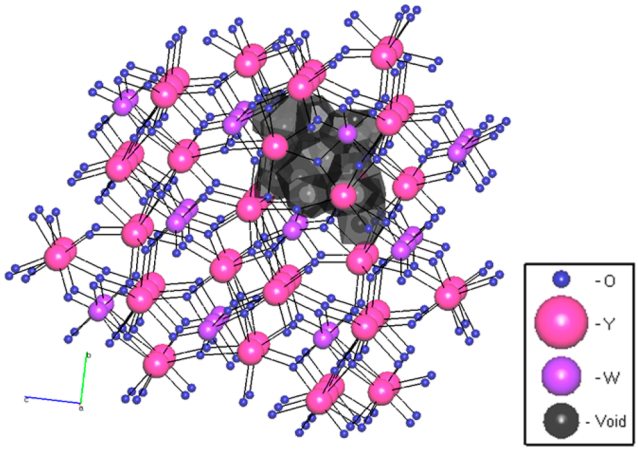

Figure 9. Representative example of a crystal structure (of $Y_2(WO_6)$ [ICSD ref 65811[91]]) bearing the most common (n = 9) n-nodal net that contains cages with suitable void-space volumes (black/gray) to accommodate PuO_2.

Cs^+ Ions. The occupational volume for Cs^+ ions was also obtained from the Slater radius[44] parameter in TOPOS, resulting in a target void-space volume of 74−78 Å^3. For this range, suitable cages in four previously reported (3 × 1°; 1 × 2°) and four predicted (3 × 1°; 1 × 2°) structures were identified (Figure 12). Figure 13 illustrates a representative example of a host structure bearing the most common n-nodal set (n = 6) that features suitable cages to contain Cs^+ ions.

Sr^{2+} Ions. The occupancy volume for Sr^{2+} ions (33.51 Å^3) was obtained from the Slater empirical radius[44] in TOPOS. Void-space volume requirements for Sr^{2+} ions generated a targeted void-space volume of 34−38 Å^3. Within this range, the suitable cages of 20 previously reported structures bearing 25 cages (5 × 1°; 7 × 2°; 13 × 3°+; 3 × multiple cages), five predicted (1 × 1°; 1 × 2°; 3 × 3°+), and one new crystal structure ((**2**), bearing a 3° cage) were identified (Figure 14). A representative example structure that bears a 3-nodal net, the most common type of host framework whose cages appear suited to accommodate Sr^{2+} ions, is shown in Figure 15.

Alternative Energy Storage. *CH_4 Molecules.* A target void-space volume of 29−33 Å^3 for methane was obtained from a kinetic diameter of 3.8 Å.[49] This resulted in the selection of 41 cages from 33 previously reported structures (14 × 1°; 7 × 2°; 20 × 3+°; 7 × multiple cages), 9 cages from 8 predicted structures (2 × 1°; 2 × 2°; 5 × 3+°; 1 × multiple cage), and a 1° cage in the newly determined structure of (**3**). Figure 16 summarizes these trends. A representative example structure, bearing the most common type of n-nodal net (n = 3) whose cages appear to be able to host CH_4 molecules, is shown in Figure 17.

H_2 Molecules. The target volume of H_2 was determined using a kinetic diameter of 2.89 Å,[19] resulting in a target void-space volume range of 13−17 Å^3. A total of 190 suitable cages to host H_2 were found in 124 previously reported structures (48 × 1°; 39 × 2°; 103 × 3°+; 39 × multiple cages), 39 cages in 23 predicted structures (4 × 1°; 5 × 2°; 30 × 3°+; 11 × multiple cages), and the in-house determined crystal structure (**3**) (4°), as shown in Figure 18. Interestingly, eight of the previously reported, as well as one of the predicted structures, each contain at least four suitable types of cages for hosting H_2. Figure 19 displays a representative example of a tungstate-based framework structure bearing the most common n-nodal set (n = 3) with suitable cages to host H_2 molecules.

General Trends. *Topological Patterns and Frequency Trends in Guest−Host Matching Preferences.* One of the main objectives of this study was the discovery of potential trends in topological patterns of tungstate framework structures with respect to their desired guest type. The results of the

DOI: 10.1021/acssuschemeng.5b00369
ACS Sustainable Chem. Eng. 2015, 3, 2112−2129

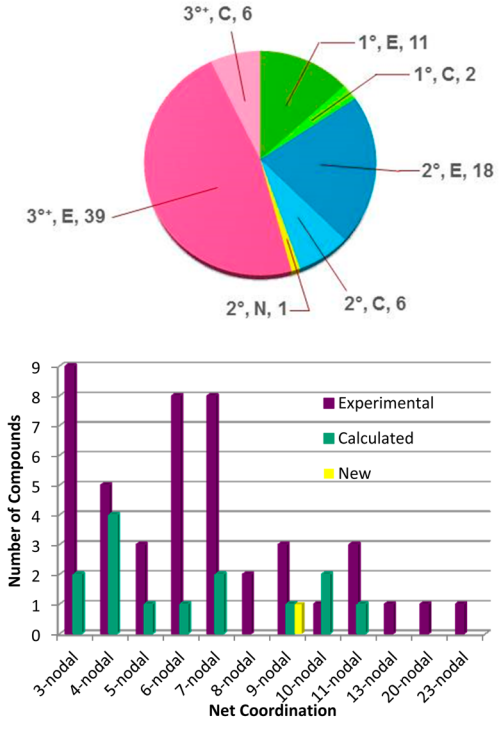

Compound	Cage attribute	Ref. [ICSD - paper]
$KLu(WO_4)_2$	E, 1°	172510 - [95]
$KYb(WO_4)_2$	E, 1°	280877 - [96]
$KEr(WO_4)_2$	E, 1°	157832 - [97]
$KY(WO_4)_2$	E, 1°	411285 - [98]
$KHo(WO_4)_2$	E, 1°	182626 - [99]
$Sr_2(CuWO_6)$	E, 1°	99303 - [100]
$Li_2Cu(WO_4)2$	E, 1°	92854 - [101]
$Li_2Ni(WO_4)_2$	E, 1°	92853 - [101]
$Li_2Co(WO_4)_2$	E, 1°	92852 - [101]
$Ce_{10}W_{22}O_{81}$	E, 1° - 3°	260095 - [81]
Bi_2WO_6	E, 1° - 3°	171328 - [102]
$Dy_2(WO_4)_3$	E, 2°	98102 - [103]
$Eu_2(WO_4)_3$	E, 2°	15877 - [104]
$Pb_3(WO_5)Cl_2$	E, 2°	89833 - [77]
$Pr_3(WO_6)Cl_3$	E, 2°	20626 - [105]
$La_3WO_6Cl_3$	E, 2°	35595 - [106]
$Rb_{12}(Nb_{30}W_3O_{90})$	E, 2°	1505 - [107]
$LiY(W_2O_8)$	E, 2°	156989 - [108]
$ErBi(W_2O_9)$	E, 2°	183443 - [72]
$EuBi(W_2O_9)$	E, 2°	183444 - [72]
$SmBi(W_2O_9)$	E, 2°	183445 - [72]
$Ca_4(Al_6O_{12})(WO_4)$	E, 2°	28481 - [109]
$Na_2(W_2O_7)$	E, 2°	1883 - [32]
$Sr_4(Al_6O_{12})(WO_4)$	E, 2°	28483 - [109]
UW_3O_{11}	E, 2°	81983 - [75]
$Ba_3WO_5Cl_2$	E, 2° - 3°	63518 - [89]
$CuSm(W_2O_8)$	E, 2° - 3°	68615 - [79]
$CuGd(W_2O_8)$	E, 3°	75006 - [110]
$LiPr(WO_4)_2$	E, 3°	200520 - [111]
$CuDy_5(WO_4)_8$	E, 3°	380067 - [112]
$Tl_2(WO_4)$	E, 3°	8212 - [80]
$Rb_2(WO_4)$	E, 3°	183200 - [113]
$Rb(NbW_2O_9)$	E, 3°	246143 - [114]
$Al_2(WO_4)_3$	E, 3° - 5°	73878 - [85]
$Al_2(WO_4)_3$	E, 3° - 5°	90936 - [86]
$FeCe(WO_4)(W_2O_8)$	E, 4° - 5°	401919 - [83]
$U(WO_4)$	E, 4° - 5°	2285 - [115]
$Al_2(WO_4)_3$	E, 4° - 8°	56827 - [85]
$Li_2(WO_4)$	E, 5° - 6°	160721 - [116]
$Li_2(WO_4)$	E, 5° - 6°	15395 - [117]
$Sc_2(WO_4)_3$	E, 6°	28467 - [118]
$In_2(WO_4)_3$	E, 6°	99606 - [119]
$Ba_2P_8W_{32}O_{112}$	E, 7° - 9°	202484 - [120]
$Al_2(WO_4)_3$	E, 8° - 10°	73879 - [85]
$(Na_2WO_4)(H_2O)_2$	E, 9°	240882 - [93]
$Na_2W_2O_7$	N, 2°	This work – [(3)]
Na_2WO_4	C, 1°	
Na_2WO_4	C, 1°	
Na_4WO_5	C, 2°	
Na_2WO_4	C, 2°	
$Na_2W_2O_7$	C, 2°	
$Na_2W_2O_7$	C, 2°	
$Na_2W_2O_7$	C, 2°	
$Na_2Al_2WO_7$	C, 2° - 3°	
Na_2WO_4	C, 3°	
$Na_2W_2O_7$	C, 3°	
$Na_2W_2O_7$	C, 3°	
$NaAlW_2O8$	C, 3°	
$Na_2W_2O_7$	C, 8°	

Figure 10. (Left) Distribution of cage types (1°, 2°, 3°+) of host structures comprising n-nodal nets that can incorporate U or Pu ions, according to their frequency observed in previously reported (E) or newly determined (N) experimental and calculated (C) crystal structures. (Right) List of their associated compound identifiers (ICSD number and ref citation).

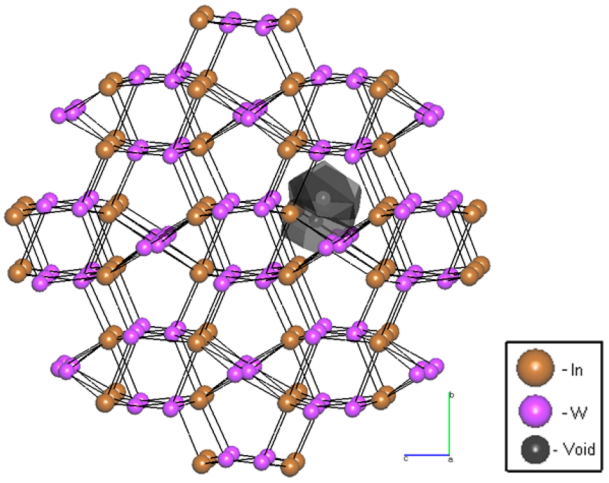

Figure 11. Representative example of a crystal structure (of $In_2(WO_4)_3$ [ICSD ref 99606[119]]) featuring the most common (n = 3) n-nodal net that bears cages with suitable void-space volumes (black/gray) to contain U or Pu ions.

experimentally determined structures clearly demonstrate that for smaller (H_2, U, or Pu) and medium-sized (CH_4 or Sr^{2+}) guests, compounds with 3-nodal nets are the most abundant. In this context, the small guest molecule CO_2 is an exception since it prefers 5- and 6-nodal structures. Within each of the predominant net classifications, the majority of the best suited cages for guests were found to be 3°, aside from those involving the two smallest guest types. Here, CO_2 is best hosted almost exclusively in 1°, 2°, or 3° cages of 5- or 6-nodal nets, whereas H_2 finds suitable host accommodation predominantly in the 1° cages of 3-nodal nets. It transpires that the three largest guests, PuO_2, UO_2, and Cs^+, prefer higher-nodal nets, and they can be hosted exclusively in 1° cages within their preferred n-nodal nets.

In contrast, computationally derived structures indicate that tungstate frameworks with higher-order nodal nets are preferred hosts, and several guest types (CO_2, H_2, CH_4) showed promise for their inclusion into 11-nodal net structures. The preferred hosts for U and Pu ions were 4-nodal nets, whereas Cs^+ preferred 6-nodal nets. For PuO_2 and UO_2, only one calculated structure, featuring an 8-nodal and a 10-nodal net, respectively, was deemed a suitable host, while Sr^{2+} guests did not exhibit any dominant net-type for their host structures.

Experimentally Derived versus Hypothetical Tungstates Structures: Trends and Biases. This discrepancy in host–guest

DOI: 10.1021/acssuschemeng.5b00369
ACS Sustainable Chem. Eng. 2015, 3, 2112–2129

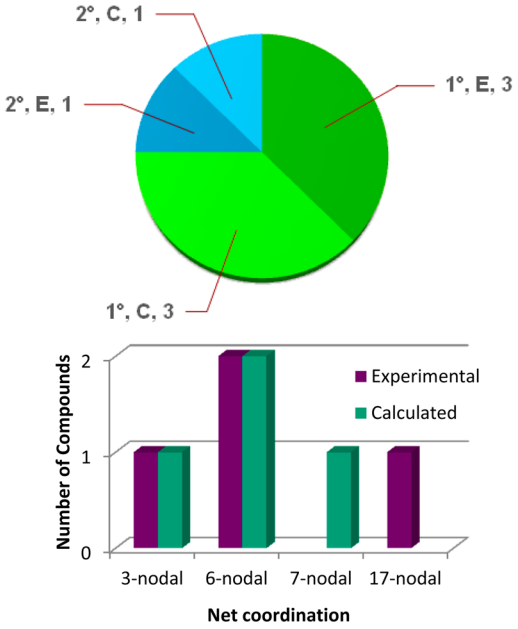

Compound	Cage attribute	Ref. [ICSD - paper]
$Gd(WO_4)Cl$	E, 1°	35292 - [39]
$Ca_2Ni(WO_6)$	E, 1°	160109 - [121]
$Li_2(WO_4)$	E, 1°	10479 - [122]
$Ca_8(Al_{12}O_{24})(WO_4)_2$	E, 2°	71806 - [123]
$Na_2W_2O_7$	C, 1°	
$NaAlW_2O_8$	C, 1°	
$NaAlW_2O_8$	C, 1°	
$NaAlW_2O_8$	C, 2°	

Figure 12. (Left) Distribution of cage types (1°, 2°) of host structures comprising n-nodal nets that can incorporate Cs^+ ions, according to their frequency observed in experimental (E) and calculated (C) crystal structures. (Right) List of their associated compound identifiers (ICSD number and ref citation).

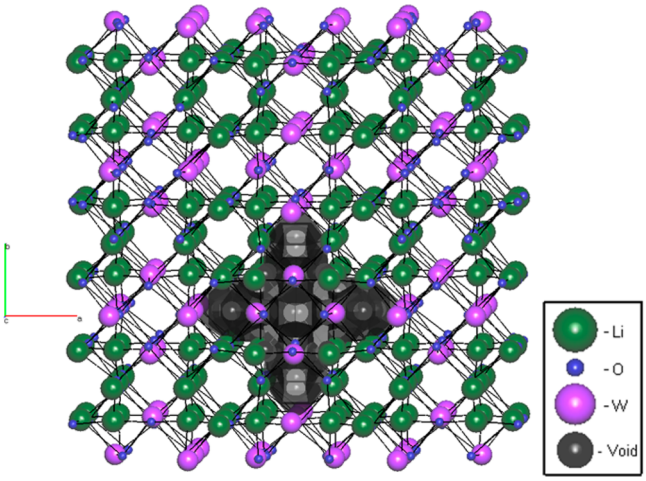

Figure 13. Representative example of a crystal structure (of $Li_2(WO_4)$ [ICSD ref 10479[122]]) displaying the most common (n = 6) n-nodal net in which cages with suitable void-space volumes (black/gray) reside to contain Cs^+ ions.

matching preferences between predicted- and experimentally determined structures may arise from a variety of factors. First, this is a rather complicated comparison given that the computationally determined hypothetical structures exclusively considered possible variations of $Na_aAl_bW_cO_d$ (where a, c, d may be any integer and b may be any integer or zero), whereas the generated set of experimentally determined structures was far less restrictive, including any structure that contains W, O, and one or two other elements. The host−guest matching preferences determined using the computationally derived structural set might naturally be refined if hypothetical tungstate structures were generated for all of the possible chemical compositions that are accepted in the experimentally derived structural set, although such a quest would be computationally expensive and laborious. So turning this problem on its head, if all compounds with the general formula $Na_aX_bW_cO_d$ (where X is any element) are isolated from the experimentally derived structural data set, a preference trend toward nets of higher order—mostly 5-, 8-, and 9-nodal nets—can be observed, i.e., experimental and computational results apparently tend toward a common preference of higher-order nodal nets as suitable hosts. However, with one exception, these trends have to be considered with caution, owing to the very limited numbers of compounds available for each guest type as a result of this data restriction. The exception concerns the set of possible hosts for H_2; in this case, 3-nodal nets remained preferred for both the full experimental findings and within this experimental source restriction to $Na_aX_bW_cO_d$.

Second, this host−guest matching preference discrepancy may be due to the generated cage volumes in the theoretically calculated structures, which were typically larger than those encountered in experimentally determined structures. Nonetheless, observed differences are cage size and type dependent. For example, primary cages for the largest cage sizes compare well between hypothetically and experimentally generated structures (329.35 and 332.79 $Å^3$, respectively). Discord appears more at the detailed level, and this reflects more of a classification problem than a straightforward difference between theory and experiment. This can be illustrated by a consideration of some primary cage statistics. If these primary cage sizes are separated into volume ranges, and a percentage is constructed for the number of primary cages found in each volume range versus the total number of primary cages, differences become more apparent. In this respect, experimental structures have 8% of primary cages in the >100 $Å^3$ range, 16% within 50−100 $Å^3$, 31% within 20−50 $Å^3$, and 45% <20 $Å^3$. In contrast, calculated structures have 35% of primary cages in the >100 $Å^3$ range, 23% within 50−100 $Å^3$, 33% within 20−50 $Å^3$, and 9% <20 $Å^3$. In addition, a greater number of distinct cages were found in many cases for the theoretically calculated structures. Again, some statistics are helpful for explanation: 62.3% of experimental structures possess 1−10 total cages, 24.3% have 11−20 total cages, 8.1% have 21−30 total cages,

DOI: 10.1021/acssuschemeng.5b00369
ACS Sustainable Chem. Eng. 2015, 3, 2112−2129

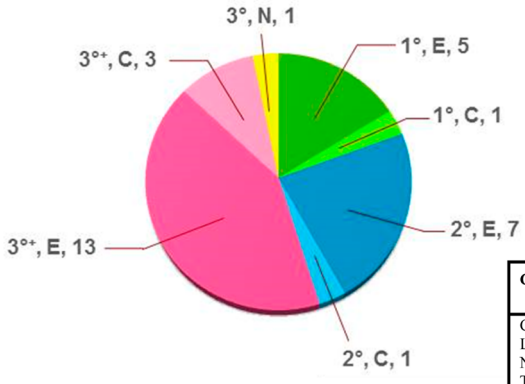

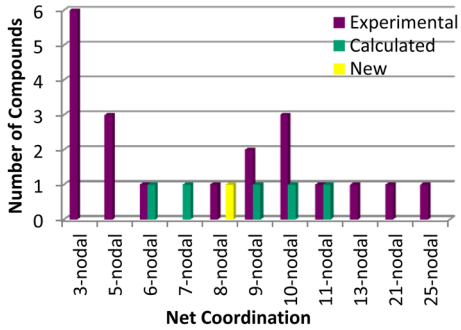

Compound	Cage attribute	Ref. [ICSD - paper]
$CuGd(W_2O_8)$	E, 1°	75006 - [110]
$LiY(W_2O_8)$	E, 1°	156989 - [108]
$Na_5La(WO_4)_4$	E, 1°	20427 - [63]
$Tl_2(WO_4)$	E, 1°	8212 - [80]
$(Bi_2O_2)(W_2O_7)$	E, 1°	88428 - [124]
$CuEr(WO_4)_2$	E, 2°	73747 - [78]
$Rb(NbW_2O_9)$	E, 2°	246143 - [114]
$CuDy_5(WO_4)_8$	E, 2°	380067 - [112]
$Rb_2(WO_4)$	E, 2°	183200 - [113]
$Sc_2(WO_4)_3$	E, 2°	28467 - [118]
$In_2(WO_4)_3$	E, 2°	99606 - [119]
$CuDy(WO_4)_2$	E, 2°- 3°	73749 - [78]
$Cu_2(WO_4)$	E, 3°	202669 - [82]
$Li_2(WO_4)$	E, 3°	160721 - [116]
$Y_2(WO_4)_3$	E, 3°	90938 - [86]
$Ag_{26}I_{18}(WO_4)_4$	E, 3°	56852 - [87]
$Al_2(WO_4)_3$	E, 3°- 4°	73879 - [85]
$(Na_2WO_4)(H_2O)_2$	E, 5°	240882 - [93]
$In_2(WO_4)_3$	E, 6° - 8°	99607 - [119]
$Zr(WO_4)_2$	E, 7°	56566 - [125]
$NaAlW_3O_{11}$	N, 3°	This work – [(**2**)]
$Na_2W_2O_7$	C, 1°	
$Na_2W_2O_7$	C, 2°	
$Na_2W_2O_7$	C, 3°	
$NaAlW_2O_8$	C, 4°	
$Na_2W_2O_7$	C, 6°	

Figure 14. (Left) Distribution of cage types (1°, 2°, 3°, 3°+) of host structures comprising n-nodal nets that can incorporate Sr^{2+} ions, according to their frequency observed in previously reported (E) or newly determined (N) experimental and calculated (C) crystal structures. (Right) List of their associated compound identifiers (ICSD number and ref citation).

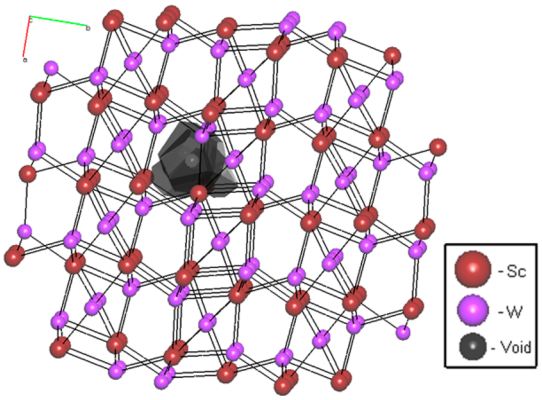

Figure 15. A representative example of a crystal structure (of $Sc_2(WO_4)_3$ [ICSD ref 28467[118]]) manifesting the most common (n = 3) n-nodal net that contains cages with suitable void-space volumes (black/gray) to accommodate Sr^{2+} ions.

4.2% have 31−40 total cages, 0.7% have 41−50 total cages, and 0.4% have >50 total cages. In contrast, 18.6% of calculated structures have 1−10 total cages, 39.5% have 11−20 total cages, 14.0% have 21−30 total cages, 9.3% have 31−40 total cages, 2.3% have 41−50 total cages, and 16.3% have >50 total cages. Furthermore, despite comprising a higher absolute number of cages, often fewer cages of distinct volumes were found for the calculated relative to the experimental structures owing to many cages numerically producing the same volume as other cages within a single structure.

Third, databases of experimentally determined crystal structures contain an intrinsic chemical bias since the determination of a crystal structure is predicated on a systematic distortion of chemical space on several accounts. For example, some classes of chemicals are easier to crystallize than others, and obtaining crystals of a compound naturally facilitates its likelihood of associated crystal structure determination. Certain families of compounds will also appear in a crystal structure database with greater frequency than others or even exist in duplicate or manifold. Possible causes of this include synthetic efforts being prolific in a specific area of chemistry where compounds are in vogue for a popular application or the prevalence of polymorphism in a series of chemicals that issues duplicate chemical structures that bear different space groups.

In the context of the subject study, this chemical bias could manifest as clusters of preferred nets owing to the large grouping of chemical families with similar structures. Indeed, such clustering is borne out in this study. One example of it features in the list of "ideal net" compounds that could host H_2, which includes five compounds with the formula $LiXW_2O_8$ (X = lanthanide). These families of compounds will naturally form similar nets, as their chemical connectivity is similar. Another example concerns the possible hosts for CH_4, among which four different space groups of $Al_2(WO_4)_3$ can be found: *Pbcn*, *Pnca*, $P2_1/n$, and $P2_1$, i.e., the replication of chemical formula but distinguished by polymorphism. Again, all of these result in the same, or similar, nets.

While computationally derived structural data sets also have the ability to feature chemical bias, such bias would have to be generated by the user, and good practice in computational research is usually able to circumvent any significant biases at the level of those present in large sets of experimental data.

DOI: 10.1021/acssuschemeng.5b00369
ACS Sustainable Chem. Eng. 2015, 3, 2112−2129

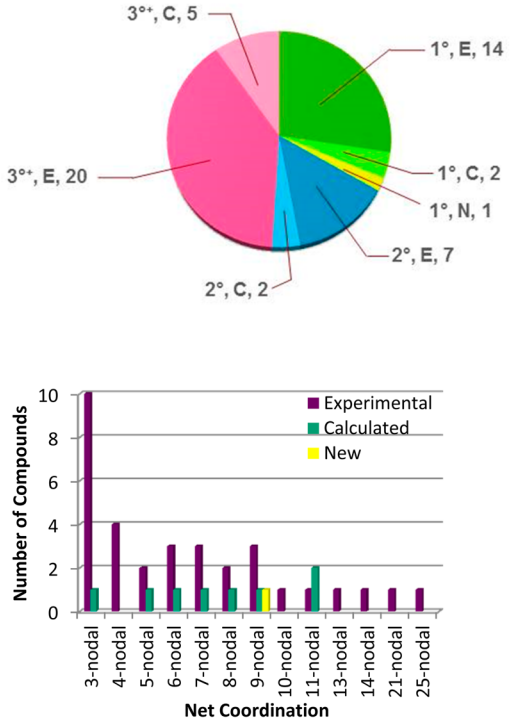

Compound	Cage attribute	Ref. [ICSD - paper]
$CsLiWO_4$	E, 1°	14082 - [126]
$RbGd(WO_4)_2$	E, 1°	152962 - [127]
$KBi(WO_4)_2$	E, 1°	391361 - [128]
$RbNd(WO_4)_2$	E, 1°	155378 - [129]
$K_2(UO_2)(W_2O_8)$	E, 1°	96443 - [130]
$Na_5Tb(WO_4)_4$	E, 1°	20426 - [63]
$Hg(WO_4)$	E, 1°	169667 - [65]
$Li_2(UO_2)_4(WO_4)_4O$	E, 1°	99481 - [131]
$Li_2(WO_4)$	E, 1°	14196 - [132]
Y_2WO_6	E, 1°	261479 - [133]
$K_2(W(O_2)_4)$	E, 1°	202672 - [134]
$Na_2(W_2O_7)$	E, 1°	1883 - [32]
$K_2W_4O_{13}$	E, 1°	2412 - [67]
$Ca_8(Al_{12}O_{24})(WO_4)_2$	E, 1°	62988 - [135]
$U(WO_4)$	E, 2°	2285 - [115]
Cu_2WO_4	E, 2°	62058 - [76]
$Bi_2(WO_6)$	E, 2°	67647 - [136]
$Al_2(WO_4)_3$	E, 2°	73878 - [85]
$La_2(WO_4)_3$	E, 2°	78180 - [137]
$Al_2(WO_4)_3$	E, 2°	90936 - [86]
$(Bi_2O_2)(W_2O_7)$	E, 2° - 3°	88428 - [124]
$CuEr(WO_4)_2$	E, 3°	73747 - [78]
$Rb_4H_8(H_2W_{12}O_{40})(H_2O)_{18}$	E, 3°	16468 - [138]
$Li_2(WO_4)$	E, 3°	15395 - [117]
$Al_2(WO_4)_3$	E, 3°	56827 - [85]
$Sc_2(WO_4)_3$	E, 3° - 4°	28467 - [118]
$In_2(WO_4)_3$	E, 3° - 4°	99606 - [119]
$Cu_2(WO_4)$	E, 4°	202669 - [82]
$Y_2(WO_4)_3$	E, 4° - 5°	90938 - [86]
$Ag_{26}I_{18}(WO_4)_4$	E, 5°	56852 - [87]
$Al_2(WO_4)_3$	E, 5° - 7°	73879 - [85]
$(Na_2WO_4)(H_2O)_2$	E, 6° - 7°	240882 - [93]
$Zr(WO_4)_2$	E, 8° - 9°	56566 - [125]
$Na_2W_2O_7$	N, 1°	This work – [(3)]
Na_2WO_4	C, 1°	
$Na_2W_2O_7$	C, 1°	
$NaAlW_2O_8$	C, 2°	
$NaAlW_2O_8$	C, 2°	
$Na_2W_2O_7$	C, 4°	
$Na_2W_2O_7$	C, 5°	
$NaAlW_2O_8$	C, 5° - 6°	
$Na_2W_2O_7$	C, 7°	

Figure 16. (Left) Distribution of cage types (1°, 2°, 3°+) of host structures comprising n-nodal nets that can incorporate CH_4 molecules, according to their frequency observed in previously reported (E) or newly determined (N) experimental and calculated (C) crystal structures. (Right) List of their associated compound identifiers (ICSD number and ref citation).

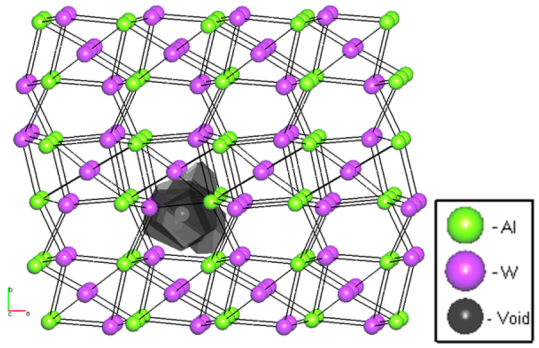

Figure 17. Representative example of a crystal structure (of $Al_2(WO_4)_3$ [ICSD ref 90936[86]]) illustrating the most common n-nodal (n = 3) net in which cages with suitable void-space volumes (black/gray) can host CH_4 molecules.

This experimental bias therefore augments the level of discrepancy between experimental and computationally derived host−guest matching preferences.

*How Do the In-House Determined Crystal Structures (**1**)−(**3**) Rate as Potential Hosts and Present within the Broader Set of Tungstate Structural Frameworks?* The in-house determined crystal structure of (**1**) contained only two cages: one relatively large (66.03 Å^3) and a relatively small one (5.28 Å^3). These cages were only able to accommodate one of the guest types (UO_2) explored in this study. The crystal structure of (**1**) represents the first report of its structural type for the formula, $NaAlW_2O_8$. Hypothetical structures that conformed to the same formula but exhibited different frameworks were nonetheless identified, and when taken collectively, they were predicted to be able to accommodate all but two guest types (PuO_2 and UO_2).

Void-space analysis indicates that the crystal structure of (**2**) can accommodate PuO_2, UO_2, or Sr^{2+}. The rarity of this crystal structure is even more stark than that of (**1**), being the first report of any structural type with formula, $NaAlW_3O_{11}$. The fact that not even any hypothetical structures of this formula were predicted via the computational aspect of this study is particularly interesting. As noted earlier, the fundamental strategy behind the structure prediction method used herein is based on the statistical likelihood of ionic substitution of previously reported crystal structures. The lack of any hypothetical structures of this formula in its prediction set is therefore symptomatic of no other previously reported experimental structures of this formula well beyond just tungstates. It would thus seem that the crystal structure of (**2**) is rare indeed, to the extent that it could now be used as an exemplar to help ionic substitution methods start to predict isomorphous structures of other (nontungstate) inorganic frameworks. The structure determination of (**2**) was in fact particularly challenging, and so the use of this first structural exemplar in concert with this type of structural prediction method could go one step further by offering computation the possibility to help guide the experimental crystallographer to probable solutions of isomorphous structures. An example of such a concerted approach, whose premise is built upon similar lines, is that of Meredig and Wolverton.[185]

Among the three in-house determined crystal structures, (**3**) offers the most options for hosting the guests explored in this study being able to accommodate U or Pu ions as well as CH_4 and H_2 molecules. In addition, the corresponding hypothetical structures of $Na_2W_2O_7$ were able to host all guests, except for PuO_2, in at least one manifestation of this chemical formula. It is worth remembering that the room-temperature crystal structure of (**3**) has been reported previously, so statistical

DOI: 10.1021/acssuschemeng.5b00369
ACS Sustainable Chem. Eng. 2015, 3, 2112−2129

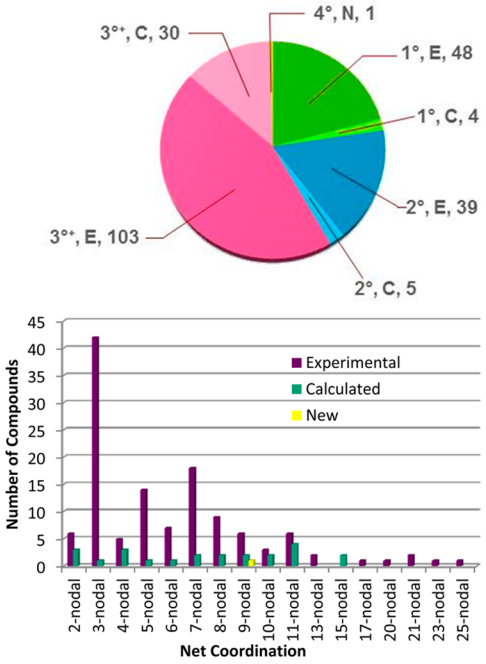

Compound	Cage attribute	Ref. [ICSD -paper]
$Li(NbWO_6)$	E, 1°	202779 - [139]
$Li(NbWO_6)$	E, 1°	202780 - [139]
$K((SbW)O_6)$	E, 1°	181570- [140]
$Cs(SbWO_6)$	E, 1°	165063 - [141]
$KNb(WO_6)$	E, 1°	63562- [142]
$AgIn(WO_4)_2$	E, 1°	60373- [143]
$LiLaW_2O_8$	E, 1°	261829- [144]
$LiGdW_2O_8$	E, 1°	261833- [144]
$LiSmW_2O_8$	E, 1°	261831 - [144]
$LiEuW_2O_8$	E, 1°	261832 - [144]
$LiNdW_2O_8$	E, 1°	261830 - [144]
$Cs(TaWO_6)$	E, 1°	165061- [141]
$NaBi(WO_4)_2$	E, 1°	168136- [145]
$Pb_2Co(WO_6)$	E, 1°	77912 - [146]
$Sr_2Zn(WO_6)$	E, 1°	72811 - [147]
$Sr_2Mg(WO_6)$	E, 1°	152575 - [148]
$Ba_2(CoWO_6)$	E, 1°	97029 - [149]
Ba_2CoWO_6	E, 1°	27425 - [150]
Ba_2NiWO_6	E, 1°	27426 - [150]
$Ba_2(FeWO_6)$	E, 1°	95520 - [151]
$Pb_2Mg(WO_6)$	E, 1°	67880 - [152]
Ba_2ZnWO_6	E, 1°	423034 - [153]
$Ba_2Ca(WO_6)$	E, 1°	245599 - [154]
$NaIn(WO_4)_2$	E, 1°	16263 - [155]
$Ni(WO_4)$	E, 1°	16685 - [156]
$CrWO_4$	E, 1°	36213 - [157]
$Ca(WO_4)$	E, 1°	155424 - [158]
$Ca(WO_4)$	E, 1°	155423 - [158]
$NaIn(WO_4)_2$	E, 1°	28098 - [159]
$Sr(WO_4)$	E, 1°	155425 - [158]
$Pb(WO_4)$	E, 1°	155522 - [160]
$Ba(WO_4)$	E, 1°	155513 - [160]
$Pb_2Co(WO_6)$	E, 1°	72905 - [161]
Ba_2MgWO_6	E, 1°	423033 - [153]
$Na_2(WO_4)$	E, 1°	44524 - [162]
$Hg(WO_4)$	E, 1°	169671 - [65]
$Nd(WO_3N)$	E, 1° - 2°	99740 - [163]
$NaDy(WO_4)_2$	E, 1° - 2°	248012 - [164]
$NaBi(WO_4)_2$	E, 1° - 2°	83318 - [165]
$NaNd(WO_4)_2$	E, 1° - 2°	66091 - [166]
$NaGd(WO_4)_2$	E, 1° - 2°	157390 - [167]
$NaLa(WO_4)_2$	E, 1° - 2°	66090 - [166]
$Pb(WO_4)$	E, 1° - 2°	75981 - [168]
$(LiLa)(WO_4)_2$	E, 1° - 2°	184015 - [169]
$Sr(WO_4)$	E, 1° - 3°	155426 - [158]
$Pb(WO_4)$	E, 1° - 3°	155518 - [160]
$Na_2ZrW_3O_{12}$	E, 1° - 3°	20405 - [170]
$Eu_3(BWO_9)$	E, 1° - 4°	39810 - [171]
$KLa(WO_4)_2$	E, 2°	95541 - [172]
$CsLu(WO_4)_2$	E, 2°	202270 - [173]
$KEu(WO_4)_2$	E, 2°	173634 - [53]
$KLu(WO_4)_2$	E, 2°	172510 - [95]
$KYb(WO_4)_2$	E, 2°	280877 - [96]
$KEr(WO_4)_2$	E, 2°	157832 - [97]
$KY(WO_4)_2$	E, 2°	411285 - [98]
$KHo(WO_4)_2$	E, 2°	182626 - [99]
$Ba(TeW_2O_9)$	E, 2°	281502 - [174]
$La_3(BWO_9)$	E, 2°	39809 - [171]
$Eu_3(BWO_9)$	E, 2°	150338 - [175]
$Dy_3(BWO_9)$	E, 2°	250419 - [55]
$Tb_3(BWO_9)$	E, 2°	250418 - [55]
$Gd_3(BWO_9)$	E, 2°	250417 - [55]
$Nd_3(BWO_9)$	E, 2°	250415 - [55]
$Sm_3(BWO_9)$	E, 2°	250416 - [55]
$Pr_3(BWO_9)$	E, 2°	250414 - [55]
$KBi(WO_4)_2$	E, 2°	391361 - [128]
$La_2(WO_4)(Te_3O_7)_2$	E, 2°	249538 - [58]
$Ba_{11}(W_4O_{23})$	E, 2°	418207 - [56]
Y_2WO_6	E, 2°	261479 - [133]
$K_5(TeW_3O_{12})$	E, 2°	97506 - [176]
$Rb_2(W_2O_7)$	E, 2°	300230 - [177]
$Hg(WO_4)$	E, 2°	169667 - [65]
LiW_3O_9	E, 2° - 3°	38310 - [178]
$Li_2(UO_2)(WO_4)_2$	E, 2° - 3°	99480 - [131]

Compound	Cage attribute	Ref. [ICSD - paper]
$NdNa_5(WO_4)_4$	E, 2°- 4°	6145 - [179]
$BiLaWO_6$	E, 3°	416793 - [52]
$BiNdWO_6$	E, 3°	416789 - [52]
$Pr_3(WO_6)Cl_3$	E, 3°	20626 - [105]
$La_3WO_6Cl_3$	E, 3°	35595 - [106]
$LiY(W_2O_8)$	E, 3°	156989 - [108]
$KNd(WO_4)_2$	E, 3°	9364 - [180]
$Ca_3WO_5Cl_2$	E, 3°	2335 - [181]
$Li_2(UO_2)_4(WO_4)_4O$	E, 3°	99481 - [131]
$Nd(WO_4)(OH)$	E, 3°	27731 - [182]
$Pb_6B_2WO_{12}$	E, 3°	261534 - [183]
$Rb_2(TeW_3O_{12})$	E, 3°	97507 - [176]
$K_2(UO_2)(W_2O_8)$	E, 3° - 5°	96443 - [130]
$Li_2Cu(WO_4)_2$	E, 3° - 5°	92854 - [101]
$Na_4Th(WO_4)_4$	E, 3° - 5°	422185 - [61]
$Li_2Ni(WO_4)_2$	E, 3° - 5°	92853 - [101]
$Li_2Co(WO_4)_2$	E, 3° - 6°	92852 - [101]
$Na_2W_2O_7(H_2O)$	E, 3° - 6°	408189 - [184]
$Na_3F(WO_4)$	E, 4°	417289 - [73]
$Rb_4H_8(H_2W_{12}O_{40})(H_2O)_{18}$	E, 4°	16468 - [138]
$Na_2(W_2O_7)$	E, 4°	1883 - [32]
$K_2W_4O_{13}$	E, 4°	2412 - [67]
$Ca_6(Al_{12}O_{24})(WO_4)_2$	E, 4°	71806 - [123]
UW_2O_{11}	E, 4°	81983 - [75]
$ErBi(W_2O_9)$	E, 4° - 5°	183443 - [72]
$EuBi(W_2O_9)$	E, 4° - 5°	183444 - [72]
$Rb_2(WO_4)$	E, 4° - 5°	183200 - [115]
$Li_2(W_2O_7)$	E, 4° - 5°	1897 - [71]
$SmBi(W_2O_9)$	E, 4° - 5°	183445 - [72]
Bi_2WO_6	E, 4° - 6°	171328 - [102]
$Na_5Lu(WO_4)_4$	E, 4° - 7°	200930 - [62]
$Na_5Tb(WO_4)_4$	E, 4° - 7°	20426 - [63]
$Rb_{12}(Nb_{30}W_3O_{90})$	E, 5°	1505 - [107]
$CuGd(W_2O_8)$	E, 5° - 6°	75006 - [110]
$LiPr(WO_4)_2$	E, 5° - 6°	200520 - [111]
$Na_5Y(WO_4)_4$	E, 5° - 9°	417143 - [74]
$Na_5La(WO_4)_4$	E, 5° - 9°	20427 - [62]
$CuDy(WO_4)_2$	E, 6°	73749 - [78]
$CuEr(WO_4)_2$	E, 6°	73747 - [78]
$CuSm(W_2O_8)$	E, 6°	68615 - [79]
$CuLa(W_2O_8)$	E, 6° - 7°	68614 - [79]
$Al_2(WO_4)_3$	E, 7°	73878 - [85]
$Al_2(WO_4)_3$	E, 7°	90936 - [86]
$Sc_2(WO_4)_3$	E, 7°	28467 - [118]
$U(WO_4)$	E, 7° - 8°	2285 - [115]
$K_2Nb_{10}W_7O_{47}$	E, 7° - 8°	62130 - [84]
$Cu_2(WO_4)$	E, 7° - 10°	202669 - [82]
$Ce_{10}W_{22}O_{81}$	E, 8° - 10°	260095 - [81]
$Ag_{26}I_{18}(WO_4)_4$	E, 9°	56852 - [87]
$FeCe(WO_4)(W_2O_8)$	E, 9° - 10°	401919 - [83]
$Na_2W_2O_7$	N, 4°	This work – [(3)]
$NaAlW_2O_8$	C, 1°	
$NaAlW_2O_8$	C, 1° - 2°	
$NaAlW_2O_8$	C, 1° - 2°	
$NaAlW_2O_8$	C, 1° - 2°	
Na_2WO_4	C, 2°	
$Na_2W_2O_7$	C, 2° - 3°	
Na_2WO_4	C, 3°	
Na_2WO_4	C, 3°	
$Na_2W_2O_7$	C, 3°	
Na_4WO_5	C, 3° - 4°	
$Na_2W_2O_7$	C, 4°	
$Na_2W_4O_{13}$	C, 4°	
$NaAlW_2O_8$	C, 4°	
$Na_2W_2O_7$	C, 5°	
Na_2WO_4	C, 5° - 6°	
$NaAlW_2O_8$	C, 5° - 6°	
$NaAlW_2O_8$	C, 5° - 7°	
$Na_2W_2O_7$	C, 5° - 9°	
$Na_2W_4O_{13}$	C, 6°	
$NaAlW_2O_8$	C, 6°	
$NaAlWO_5$	C, 6° - 7°	
$NaAlW_2O_8$	C, 6° - 8°	
$Na_2W_2O_7$	C, 10°	

Figure 18. (Left) Distribution of cage types (1°, 2°, 3°+, 4°) of host structures comprising n-nodal nets that can incorporate H_2 molecules, according to their frequency observed in previously reported (E) or newly determined (N) experimental and calculated (C) crystal structures. (Right) List of their associated compound identifiers (ICSD number and ref citation).

inferences behind the structure prediction method used in this study are facilitated with pre-existing crystal structure evidence. The fact that (**3**) differs from (**1**) and (**2**) by its chemical lack of Al is presumably also significant to the nature of these host–guest matching preferences. In any event, the finding that (**3**) offers the most abundant selection of host–guest matching preferences among our three in-house available materials means that we now have a practical guide forward for prioritizing experimental host–guest adsorption studies on these compounds.

Concluding Remarks and Future Outlook. Void-space analysis of 577 tungstate crystal structures, mined from experimentally and computationally derived data sources, offers an important first step toward identifying new host materials for environmentally important small molecules and ions. A total of 196 hypothetical tungstate structures were generated using the recently developed structure prediction methods that exploit the statistical likelihood of ionic substitution;[38] 378 experimentally determined crystal structures of tungstates were sourced from the ICSD and coupled with three in-house crystal structure determinations of tungstate materials (**1**)–(**3**). It transpired that $NaAlW_2O_8$ (**1**) and $NaAlW_3O_{11}$ (**2**) present somewhat rare crystal structures, and while (**2**) appears well suited to host several nuclear waste materials, $Na_2W_2O_7$ (**3**) is predisposed to accommodate small molecules, CH_4 and H_2, for alternative energy applications, as well as industrially relevant ions for containing nuclear waste.

Beyond the immediate practical considerations of these three in-house available materials, the data-mining aspect of this study pinpoints a number of other tungstate framework structures that can, when taken collectively, host the entire range of environmentally important molecules and ions explored in this study (CO_2, UO_2, PuO_2, U, Pu, Cs^+, Sr^{2+}, CH_4, and H_2). To this end, these results offer good prospects for tungstate compounds as viable host materials for environmental storage applications. Some of these other tungstate

DOI: 10.1021/acssuschemeng.5b00369
ACS Sustainable Chem. Eng. 2015, 3, 2112–2129

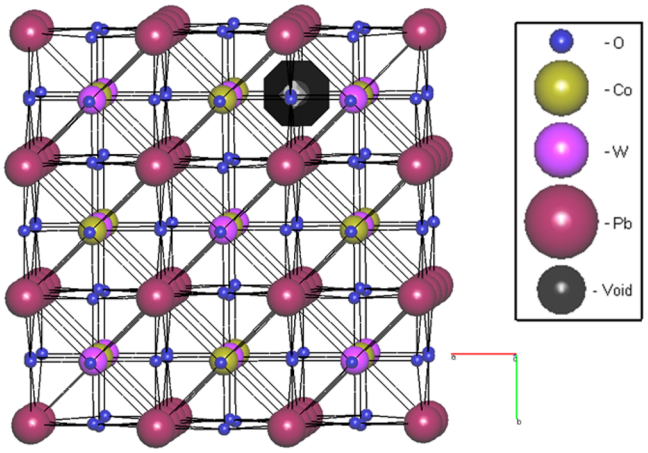

Figure 19. Representative example of a crystal structure (of $Pb_2Co(WO_6)$ [ICSD ref 72905[161]]) displaying the most common n-nodal (n = 3) net in which cages with suitable void-space volumes (black/gray) can host H_2 molecules.

structures may even host certain guests better than the in-house tungstate materials immediately available to us. However, the scope of this study essentially provides a binary outcome for a given framework structure: either the structure is, or is not, able to host a given guest. While this study illustrates a preference to certain types of n-nodal structures by virtue of their observed frequency, this does not imply directly that these preferred hosts are superior to those less commonly found. There are currently no formal ranking criteria that define one tungstate compound over another as being better able to host a given type of guest. It would be natural to develop such a ranking formalism as these void-space analysis methods continue to evolve. To this end, comparison with other host/guest prediction methods, such as channel evaluation,[26] or sub-structural similarity functions[186] might prove useful. This will further assist the experimentally minded materials scientist in selecting their host material to most optimally store small, but environmentally important, molecules or ions.

Notwithstanding the powerful practical bearing of generating a catalogue of material selections that could ultimately allow one to simply "dial up" a request to match a host structure to a desired guest, it should also be remembered that the currently predicted host frameworks have hypothetical as well as experimental crystal structure origins, so some of these tungstate materials have yet to be experimentally realized; the combined sets of experimentally and computationally generated data are also currently limited. In the spirit of considering further developments of this approach, a more explicit parametrization of guest shape may also help to refine the host–guest matching preferences predicted by this study.

Looking ahead, it should be remembered that this study has only shown how to physically fit guest types into cages of host structures; it has not considered the fabrication method of the host–guest composite. Indeed, this is a study in its own right, and much research has been engaged with studying the dynamic processes associated with adsorption of a specific guest into an individual host[187,188] or nanofabrication routes that render *in situ* host–guest synthesis where the guest is embedded into the host in a concerted fashion.[189,190] The subject study represents more of a "ship in a bottle" perspective, considering the final outcome, pending the experimental adsorption conditions (heat, pressure, reaction phase, etc.) or concerted host–guest nanofabrication methods can be resolved. Ideally, this "ship in a bottle" approach, which surveys a broad set of structures, will ultimately go hand-in-hand with simulations of adsorption dynamics or nano-fabrication of individual guest–host composites that can be short-listed via our procedure with auxiliary considerations that ensure chemical compatibility between host and guest. Creating such a unified effort will enable an "all-in-one" prediction of molecular storage capabilities and its associated synthetic processing.

■ ASSOCIATED CONTENT

Supporting Information

Crystallographic information files for (**1**–**3**). The Supporting Information is available free of charge on the ACS Publications website at DOI: 10.1021/acssuschemeng.5b00369.

■ AUTHOR INFORMATION

Corresponding Author

*E-mail: jmc61@cam.ac.uk.

Present Address

A. Zeidler: Department of Physics, University of Bath, Bath BA2 7AY, United Kingdom.

Notes

The authors declare no competing financial interest.

■ ACKNOWLEDGMENTS

Velin Nikolov from the Bulgarian Academy of Sciences is gratefully acknowledged for supplying the samples of tungstate materials (**1**)–(**3**). John J. Rickard from the Cavendish Laboratory, University of Cambridge, is thanked for his technical assistance with the EDX experiment. J.M.C. is indebted to the Fulbright Commission for a UK–US Fulbright Scholar Award hosted by Argonne National Laboratory where work done was supported by the Department of Energy, Office of Science, Office of Basic Energy Sciences, under Contract No. DE-AC02-06CH11357.

■ REFERENCES

(1) Pires, J.; Carvalho, A.; de Carvalho, M. B. Adsorption of Volatile Organic Compounds in Y Zeolites and Pillared Clays. *Microporous Mesoporous Mater.* **2001**, *43* (3), 277–287.

(2) Shu, H.-T.; Li, D.; Scala, A. A.; Ma, Y. H. Adsorption of Small Organic Pollutants from Aqueous Streams by Aluminosilicate-Based Microporous Materials. *Sep. Purif. Technol.* **1997**, *11* (1), 27–36.

(3) Millward, A. R.; Yaghi, O. M. Metal-Organic Frameworks with Exceptionally High Capacity for Storage of Carbon Dioxide at Room Temperature. *J. Am. Chem. Soc.* **2005**, *127* (51), 17998–17999.

(4) Drabarek, E.; McLeod, T. I.; Hanna, J. V.; Griffith, C. S.; Luca, V. Tungstate-Based Glass–ceramics for the Immobilization of Radio Cesium. *J. Nucl. Mater.* **2009**, *384* (2), 119–129.

(5) Luca, V.; Griffith, C. S.; Drabarek, E.; Chronis, H. Tungsten Bronze-Based Nuclear Waste Form Ceramics. Part 1. Conversion of Microporous Tungstates to Leach Resistant Ceramics. *J. Nucl. Mater.* **2006**, *358* (2–3), 139–150.

(6) Luca, V.; Drabarek, E.; Chronis, H.; McLeod, T. Tungsten Bronze-Based Nuclear Waste Form Ceramics. Part 3: The System Cs0.3MxW1−xO3 for the Immobilization of Radio Cesium. *J. Nucl. Mater.* **2006**, *358* (2–3), 164–175.

(7) Griffith, C. S.; Sebesta, F.; Hanna, J. V.; Yee, P.; Drabarek, E.; Smith, M. E.; Luca, V. Tungsten Bronze-Based Nuclear Waste Form Ceramics. Part 2: Conversion of Granular Microporous Tungstate–polyacrylonitrile (PAN) Composite Adsorbents to Leach Resistant Ceramics. *J. Nucl. Mater.* **2006**, *358* (2–3), 151–163.

DOI: 10.1021/acssuschemeng.5b00369
ACS Sustainable Chem. Eng. 2015, 3, 2112–2129

(8) Eddaoudi, M.; Kim, J.; Rosi, N.; Vodak, D.; Wachter, J.; O'Keeffe, M.; Yaghi, O. M. Systematic Design of Pore Size and Functionality in Isoreticular MOFs and Their Application in Methane Storage. *Science* **2002**, *295* (5554), 469−472.
(9) Msayib, K. J.; Book, D.; Budd, P. M.; Chaukura, N.; Harris, K. D. M.; Helliwell, M.; Tedds, S.; Walton, A.; Warren, J. E.; Xu, M.; et al. Nitrogen and Hydrogen Adsorption by an Organic Microporous Crystal. *Angew. Chem.* **2009**, *121* (18), 3323−3327.
(10) Furukawa, H.; Yaghi, O. M. Storage of Hydrogen, Methane, and Carbon Dioxide in Highly Porous Covalent Organic Frameworks for Clean Energy Applications. *J. Am. Chem. Soc.* **2009**, *131* (25), 8875−8883.
(11) Chun, H.; Moon, J. Discovery, Synthesis, and Characterization of an Isomeric Coordination Polymer with Pillared Kagome Net Topology. *Inorg. Chem.* **2007**, *46* (11), 4371−4373.
(12) Li, H.; Eddaoudi, M.; O'Keeffe, M.; Yaghi, O. M. Design and Synthesis of an Exceptionally Stable and Highly Porous Metal-Organic Framework. *Nature* **1999**, *402* (6759), 276−279.
(13) Ockwig, N. W.; Delgado-Friedrichs, O.; O'Keeffe, M.; Yaghi, O. M. Reticular Chemistry: Occurrence and Taxonomy of Nets and Grammar for the Design of Frameworks. *Acc. Chem. Res.* **2005**, *38* (3), 176−182.
(14) O'Keeffe, M.; Yaghi, O. M. Deconstructing the Crystal Structures of Metal-Organic Frameworks and Related Materials into Their Underlying Nets. *Chem. Rev.* **2012**, *112* (2), 675−702.
(15) Rosi, N. L.; Eckert, J.; Eddaoudi, M.; Vodak, D. T.; Kim, J.; O'Keeffe, M.; Yaghi, O. M. Hydrogen Storage in Microporous Metal-Organic Frameworks. *Science* **2003**, *300* (5622), 1127−1129.
(16) Tranchemontagne, D. J.; Mendoza-Cortés, J. L.; O'Keeffe, M.; Yaghi, O. M. Secondary Building Units, Nets and Bonding in the Chemistry of Metal-Organic Frameworks. *Chem. Soc. Rev.* **2009**, *38* (5), 1257−1283.
(17) Wong-Foy, A. G.; Matzger, A. J.; Yaghi, O. M. Exceptional H_2 Saturation Uptake in Microporous Metal-Organic Frameworks. *J. Am. Chem. Soc.* **2006**, *128* (11), 3494−3495.
(18) Menon, V.; Komarneni, S. Porous Adsorbents for Vehicular Natural Gas Storage: A Review. *J. Porous Mater.* **1998**, *5*, 43−58.
(19) Rowsell, J. L. C.; Yaghi, O. M. Strategies for Hydrogen Storage in Metal–Organic Frameworks. *Angew. Chem., Int. Ed.* **2005**, *44* (30), 4670−4679.
(20) Wang, B.; Côté, A. P.; Furukawa, H.; O'Keeffe, M.; Yaghi, O. M. Colossal Cages in Zeolitic Imidazolate Frameworks as Selective Carbon Dioxide Reservoirs. *Nature* **2008**, *453* (7192), 207−211.
(21) Luebbers, M. T.; Wu, T.; Shen, L.; Masel, R. I. Trends in the Adsorption of Volatile Organic Compounds in a Large-Pore Metal-Organic Framework, IRMOF-1. *Langmuir* **2010**, *26* (13), 11319−11329.
(22) Yang, K.; Sun, Q.; Xue, F.; Lin, D. Adsorption of Volatile Organic Compounds by Metal-Organic Frameworks MIL-101: Influence of Molecular Size and Shape. *J. Hazard. Mater.* **2011**, *195*, 124−131.
(23) Côté, A. P.; Benin, A. I.; Ockwig, N. W.; O'Keeffe, M.; Matzger, A. J.; Yaghi, O. M. Porous, Crystalline, Covalent Organic Frameworks. *Science* **2005**, *310* (5751), 1166−1170.
(24) Ewing, R. C. The Design and Evaluation of Nuclear-Waste Forms: Clues from Mineralogy. *Can. Mineral.* **2001**, *39* (June), 697−715.
(25) Hamdi, B.; Houari, M.; Hamoudi, S.; Kessaïssia, Z. Adsorption of Some Volatile Organic Compounds on Geomaterials. *Desalination* **2004**, *166*, 449−455.
(26) Anurova, N.; Blatov, V.; Ilyushin, G.; Blatova, O.; Ivanovschitz, A.; Demyanets, L. Migration Maps of Li^+ Cations in Oxygen-Containing Compounds. *Solid State Ionics* **2008**, *179* (39), 2248−2254.
(27) Blatov, V. A. Nanocluster Analysis of Intermetallic Structures with the Program Package TOPOS. *Struct. Chem.* **2012**, *23* (4), 955−963.
(28) *The 2007 UK Radioactive Waste Inventory: A Review of the Processes Contributing to Radioactive Wastes in the UK*; Pöyry Energy Limited, 2008.
(29) Griffith, C. S.; Luca, V. Ion-Exchange Properties of Microporous Tungstates. *Chem. Mater.* **2004**, *16* (24), 4992−4999.
(30) Forsberg, C. W. Rethinking High-Level Waste Disposal: Separate Disposal of High-Heat Radionuclides (^{90}Sr and ^{137}Cs) Management and Disposal. *Nucl. Technol.* **2008**, *131* (2), 252−268.
(31) Nikolov, I.; Nikolov, V.; Peshev, P. Regions of Phase Crystallization and New Double Tungstates in the System Na_2O−Al_2O_3−WO_3. *J. Alloys Compd.* **2003**, *351* (1−2), 202−207.
(32) Okada, K.; Morikawa, H.; Marumo, F.; Iwai, S. Disodium Ditungstate. *Acta Crystallogr., Sect. B: Struct. Crystallogr. Cryst. Chem.* **1975**, *31* (4), 1200−1201.
(33) Otwinowski, Z.; Minor, W. Processing of X-ray Diffraction Data Collected in Oscillation Mode. In *Methods in Enzymology, Vol. 276: Macromolecular Crystallography, Part A*; Carter, C. W., Jr., Sweet, R. M., Eds.; Academic Press: New York, 1997; pp 307−326.
(34) Blessing, R. H. An Empirical Correction for Absorption Anisotropy. *Acta Crystallogr., Sect. A: Found. Crystallogr.* **1995**, *51 (Pt 1)* (1), 33−38.
(35) *CrystalClear-SM Expert 2.0 software*; Rigaku Americas and Rigaku, 2009.
(36) Higashi, T. *ABSCOR*; Rigaku Corporation: Tokyo, 1995.
(37) Sheldrick, G. M. A Short History of SHELX. *Acta Crystallogr., Sect. A: Found. Crystallogr.* **2008**, *64* (1), 112−122.
(38) Hautier, G.; Fischer, C.; Ehrlacher, V.; Jain, A.; Ceder, G. Data Mined Ionic Substitutions for the Discovery of New Compounds. *Inorg. Chem.* **2011**, *50*, 656−663.
(39) Delgado-Friedrichs, O.; O'Keeffe, M. Crystal Nets as Graphs: Terminology and Definitions. *J. Solid State Chem.* **2005**, *178* (8), 2480−2485.
(40) Bonneau, C.; Delgado-Friedrichs, O.; O'Keeffe, M.; Yaghi, O. M. Three-Periodic Nets and Tilings: Minimal Nets. *Acta Crystallogr., Sect. A: Found. Crystallogr.* **2004**, *60* (6), 517−520.
(41) Blatov, V. A.; O'Keeffe, M.; Proserpio, D. M. Vertex-, Face-, Point-, Schläfli-, and Delaney-Symbols in Nets, Polyhedra and Tilings: Recommended Terminology. *CrystEngComm* **2010**, *12* (1), 44.
(42) Essam, J. W.; Fisher, M. E. Some Basic Definitions in Graph Theory. *Rev. Mod. Phys.* **1970**, *42* (2), 272−288.
(43) Blatov, V. A.; Delgado-Friedrichs, O.; O'Keeffe, M.; Proserpio, D. M. Three-Periodic Nets and Tilings: Natural Tilings for Nets. *Acta Crystallogr., Sect. A: Found. Crystallogr.* **2007**, *63* (5), 418−425.
(44) Slater, J. C. Atomic Radii in Crystals. *J. Chem. Phys.* **1964**, *41* (10), 3199.
(45) Desgranges, L.; Baldinozzi, G.; Rousseau, G.; Nièpce, J.-C.; Calvarin, G. Neutron Diffraction Study of the in Situ Oxidation of UO_2. *Inorg. Chem.* **2009**, *48*, 7585−7592.
(46) Belin, R. C.; Valenza, P. J.; Reynaud, M. A.; Raison, P. E. New Hermetic Sample Holder for Radioactive Materials Fitting to Siemens D5000 and Bruker D8 X-Ray Diffractometers: Application to the Rietveld Analysis of Plutonium Dioxide. *J. Appl. Crystallogr.* **2004**, *37* (6), 1034−1037.
(47) Taggard, J. E., Jr.; Foord, E. E.; Rosenzweig, A.; Hanson, T. Scrutinyite, Natural Occurrence of A-PbO_2 from Bingham, New Mexico, U.S.A., and Mapimi, Mexico. *Can. Mineral.* **1988**, *26*, 905−910.
(48) Kolitsch, U.; Maczka, M.; Hanuza, J. $NaAl(MoO_4)_2$: A Rare Structure Type among Layered Yavapaiite-Related $AM(XO_4)_2$ Compounds. *Acta Crystallogr., Sect. E: Struct. Rep. Online* **2003**, *59* (2), i10−i13.
(49) Sozzani, P.; Bracco, S.; Comotti, A.; Ferretti, L.; Simonutti, R. Methane and Carbon Dioxide Storage in a Porous van Der Waals Crystal. *Angew. Chem., Int. Ed.* **2005**, *44* (12), 1816−1820.
(50) Michel, C.; Groult, D.; Deschanvres, A.; Raveau, B. Proprietes D'echange D'ions Des Pyrochlores AB_2O_6—II Evolution Thermique Des Pyrochlores $AMWO_6.H_2O$ (A = Li, Na, Ag; M = Nb, Ta, Sb). *J. Inorg. Nucl. Chem.* **1975**, *37*, 251−255.

DOI: 10.1021/acssuschemeng.5b00369
ACS Sustainable Chem. Eng. 2015, 3, 2112−2129

(51) Knyazev, A. V.; Mączka, M.; Smirnova, N. N.; Macalik, L.; Kuznetsova, N. Y.; Letyanina, I. A. Crystal Structure, Spectroscopy and Thermodynamic Properties of $MIVWO_6$(MI − Li, Na). *J. Solid State Chem.* **2009**, *182*, 3003−3012.
(52) Berdonosov, P. S.; Charkin, D. O.; Knight, K. S.; Johnston, K. E.; Goff, R. J.; Dolgikh, V. A.; Lightfoot, P. Phase Relations and Crystal Structures in the Systems $(Bi,Ln)_2WO_6$ and $(Bi,Ln)_2MoO_6$ (Ln=lanthanide). *J. Solid State Chem.* **2006**, *179*, 3437−3444.
(53) Macalik, L.; Tomaszewski, P. E.; Lisiecki, R.; Hanuza, J. The Crystal Structure, Vibrational and Luminescence Properties of the Nanocrystalline $KEu(WO_4)_2$ and $KGd(WO_4)_2$:Eu^{3+} Obtained by the Pechini Method. *J. Solid State Chem.* **2008**, *181*, 2591−2600.
(54) Fu, W. T.; Au, Y. S.; Akerboom, S.; IJdo, D. J. W. Crystal Structures and Chemistry of Double Perovskites $Ba_2M(II)M'(VI)O_6$ (M=Ca, Sr, M' = Te, W, U). *J. Solid State Chem.* **2008**, *181*, 2523−2529.
(55) Krut'ko, V. A.; Belik, A. A.; Lysanova, G. V. Structures of Nonlinear Hexagonal Boratotungstates Ln_3BWO_9 (Ln= La, Pr, Nd, Sm, Gd, Tb, Dy). *Zh. Neorg. Khim.* **2006**, *51* (6), 954−959.
(56) Hong, S. T. Novel Perovskite-Related Barium Tungstate $Ba_{11}W_4O_{23}$. *J. Solid State Chem.* **2007**, *180*, 3039−3048.
(57) Lv, P.; Chen, D.; Li, W.; Xue, L.; Huang, F.; Liang, J. Subsolidus Phase Relationships in the System ZnO-Li_2O-WO_3. *J. Alloys Compd.* **2008**, *460*, 142−146.
(58) Jiang, H. L.; Ma, E.; Mao, J. G. New Luminescent Solids in the Ln-W(Mo)-Te-O-(Cl) Systems. *Inorg. Chem.* **2007**, *46* (17), 7012−7023.
(59) Brixner, L. H.; Chen, H. -y.; Foris, C. M. Structure and Luminescence of the Monoclinic $LnWO_4Cl$-Type Rare Earth Halo Tungstates. *Mater. Res. Bull.* **1982**, *17*, 1545−1556.
(60) Boulahya, K.; Parras, M.; González-Calbet, J. M. A Structural Study of the Solid Solution $Eu_2(Mo_{1-x}W_x)_3O_{12}$. *Z. Anorg. Allg. Chem.* **2005**, *631*, 1988−1990.
(61) Bang Jin, G.; Soderholm, L. Syntheses and Single-Crystal Structures of $CsTh(MoO_4)_2Cl$ and $Na_4Th(WO_4)_4$. *J. Solid State Chem.* **2011**, *184*, 337−342.
(62) Efremov, V. A.; Berezina, T. A.; Averina, I. M.; Trunov, V. K. Structure of $Na_5Tb(MoO_4)_4$, $Na_5Lu(MoO_4)_4$, and $Na_5Lu(WO_4)_4$. *Kristallografiya* **1980**, *25*, 254−261.
(63) Efremov, V. A.; Trunov, V. K.; Berezina, T. A. Fine Changes in the Structure of Scheelite-like $Na_5Tr(EO_4)_4$ with a Variation in Their Elemental Composition. *Kristallografiya* **1982**, *27*, 134−139.
(64) Grivel, J. C.; Norby, P. Subsolidus Phase Relations of the SrO-WO_3-CuO System at 800 °C in Air. *J. Alloys Compd.* **2012**, *513*, 304−309.
(65) Manjón, F. J.; López-Solano, J.; Ray, S.; Gomis, O.; Santamaría-Pérez, D.; Mollar, M.; Panchal, V.; Errandonea, D.; Rodríguez-Hernández, P.; Muñoz, A. High-Pressure Structural and Lattice Dynamical Study of $HgWO_4$. *Phys. Rev. B: Condens. Matter Mater. Phys.* **2010**, *82*, 035212−1−035212−12.
(66) Klug, A. X-Ray Diffraction Studies of Potassium Polytungstates with High WO_3 Content. *Mater. Res. Bull.* **1977**, *12*, 837−845.
(67) Okada, K.; Marumo, F.; Iwai, S. The Crystal Structure of $K_2W_4O_{13}$. *Acta Crystallogr., Sect. B: Struct. Crystallogr. Cryst. Chem.* **1978**, *34*, 3193−3195.
(68) Mormann, T. J.; Jeitschko, W. Mercury(I) Molybdates and Tungstates: Hg_2WO_4 and Two Modifications of Hg_2MoO_4. *Inorg. Chem.* **2000**, *39*, 4219−4223.
(69) Kovba, L. M.; Lykova, L. N.; Balashov, V. L.; Kharlanov, A. L. Crystal Structure of Ba_2WO_5. *Koord. Khimiya* **1985**, *11* (10), 1426−1429.
(70) Guarnieri, A. A.; Moreira, A. M.; Pinheiro, C. B.; Speziali, N. L. Structural and Calorimetric Studies of Mixed $K_2Mo_xW_{(1-x)}O_4$ ($0 \leqslant x \leqslant 1$) Compounds. *Phys. B* **2003**, *334*, 303−309.
(71) Okada, K.; Morikawa, H.; Marumo, F.; Iwai, S. The Crystal Structure of $Li_2W_2O_7$. *Acta Crystallogr., Sect. B: Struct. Crystallogr. Cryst. Chem.* **1975**, *31*, 1451−1454.
(72) Li, Y.-Y.; Cheng, W.-D.; Zhang, H.; Lin, C.-S.; Zhang, W.-L.; Geng, L.; Chai, G.-L.; Luo, Z.-Z.; He, Z.-Z. A Series of Novel Rare-Earth Bismuth Tungstate Compounds $LnBiW_2O_9$ (Ln=Ce, Sm, Eu, Er): Synthesis, Crystal Structure, Optical and Electronic Properties. *Dalton Trans.* **2011**, *40*, 7357−7364.
(73) Hartenbach, I.; Schleid, T. $Na_3F[WO_4]$: A Sodium Fluoride *Ortho*-Oxotungstate(VI) with Strands of Face-Shared Fluoride-Centred Sodium Octahedra According to $^1{}_\infty\{[FNa_{6/2}]^{2+}\}$. *Z. Anorg. Allg. Chem.* **2007**, *633*, 524−526.
(74) Hartenbach, I.; Marchetti, B.; Schleid, T. $Na_5Y[WO_4]_4$: Ein Natrium - Yttrium - Ortho-Oxowolframat Mit Einer Teraedrischen Na^+ - Koordination. *Z. Kristallogr. Suppl. Issue* **2007**, *25* (079), 22.
(75) Sundberg, M.; Marinder, B. Ordered and Defect Structures in the UO_2 − WO_3 System, Revealed by HREM. *J. Solid State Chem.* **1996**, *121*, 167−173.
(76) Marinder, B. O.; Wang, P.-L.; Werner, P. E.; Westdahl, M.; Andresen, A. F.; Louer, D. Powder Diffraction Studies of Cu_2WO_4. *Acta Chem. Scand.* **1987**, *41a*, 152−157.
(77) Grice, J. D.; Dunn, P. J. Crystal Structure Determination of Pinalite. *Am. Mineral.* **2000**, *85*, 806−809.
(78) Müller-Buschbaum, H.; Gressling, T. Zur Dimorphie von Kupfer-Lanthanoid-Oxowolframaten Am Beispiel von $CuErW_2O_8$, Mit Einem Beitrag Über $CuDyW_2O_8$. *J. Alloys Compd.* **1993**, *202*, 63−67.
(79) Boehlke, A.; Müller-Buschbaum, H. Ein Beitrag Zur Kristallstruktur von $CuLaW_2O_8$ Und $CuSmW_2O_8$. *J. Less-Common Met.* **1990**, *162*, 141−147.
(80) Okada, K.; Ossaka, J.; Iwai, S. Structure of Dithallium tungstate(VI). *Acta Crystallogr., Sect. B: Struct. Crystallogr. Cryst. Chem.* **1979**, *35*, 2189−2191.
(81) Barker, R. S.; Evans, I. R. Structural Characterization of $RE_{10}W_{22}O_{81}$ Rare-Earth Tungstates (RE = Ce, Nd). *Acta Crystallogr., Sect. B: Struct. Sci.* **2008**, *64*, 708−712.
(82) Mumm, H.-C.; Müller-Buschbaum, H. Zur Kristallstruktur von Cu_2WO_4. *J. Less-Common Met.* **1988**, *142*, 85−90.
(83) Gressling, T.; Müller-Buschbaum, H. Ein Neuer Strukturtyp Am Lanthanoid-Oxowolframat $FeCe(WO_4)W_2O_8$ = $FeCe(WO_4)_3$. *Z. Anorg. Allg. Chem.* **1996**, *622*, 254−258.
(84) Sundberg, M.; Lundberg, M. $K_x(Nb,W)_{17}O_{47}$ (1LxL2): A New Tunnel Structure Derived from High-Resolution Electron Micrographs. *Acta Crystallogr., Sect. B: Struct. Sci.* **1987**, *43*, 429−434.
(85) Hanuza, J.; Maczka, M.; Hermanowicz, K.; Andruszkiewicz, M.; Pietraszko, A.; Strek, W.; Dereń, P. The Structure and Spectroscopic Properties of $Al_{2-x}Cr_x(WO_4)_3$ Crystals in Orthorhombic and Monoclinic Phases. *J. Solid State Chem.* **1993**, *105*, 49−69.
(86) Woodcock, D. A.; Lightfoot, P.; Ritter, C. Negative Thermal Expansion in $Y_2(WO_4)_3$. *J. Solid State Chem.* **2000**, *149*, 92−98.
(87) Chan, L. Y. Y.; Geller, S. Crystal Structure and Conductivity of 26-Silver 18-Iodide Tetratungstate, $Ag_{26}I_{18}W_4O_{16}$. *J. Solid State Chem.* **1977**, *21*, 331−347.
(88) Evans, J. S. O.; Mary, T. A.; Vogt, T.; Subramanian, M. A.; Sleight, A. W. Negative Thermal Expansion in ZrW_2O_8 and HfW_2O_8. *Chem. Mater.* **1996**, *8*, 2809−2823.
(89) Spitsyn, V. I.; Balashov, V. L.; Kharlanov, A. L.; Lykova, L. N.; Kovba, L. M. Crystal Structure of $Ba_3WO_5Cl_2$. *Dokl. Akad. Nauk SSSR* **1985**, *284* (1), 125−127.
(90) Tyulin, A. V.; Efremov, V. A. Polymorphism of Oxytungstates Tr_2WO_6. Mechanism of Structural Changes of Er_2WO_6. *Kristallografiya* **1987**, *32*, 363−370.
(91) Tyulin, A. V.; Efremov, V. A.; Trunov, V. K. Polymorphism of Oxytungstates TR_2WO_6. Mechanisms of Structural Changes in Y_2WO_6. *Kristallografiya* **1989**, *34*, 885−892.
(92) Tyulin, A. V.; Efremov, V. A. Polymorphism of Oxytungstates Tr_2WO_6. Analysis of Structural Type II (Gd_2WO_6 and Gd_2MoO_6). Mechanism of Structural Change in Gd_2WO_6 in the Phase Transition II <-> V. *Kristallografiya* **1987**, *32*, 371−377.
(93) Farrugia, L. J. Sodium Tungstate Dihydrate: A Redetermination. *Acta Crystallogr., Sect. E: Struct. Rep. Online* **2007**, *63*.i14210.1107/S1600536807023355
(94) Ewing, R. C. Nuclear Waste Forms for Actinides. *Proc. Natl. Acad. Sci. U. S. A.* **1999**, *96* (7), 3432−3439.

DOI: 10.1021/acssuschemeng.5b00369
ACS Sustainable Chem. Eng. 2015, 3, 2112−2129

(95) Pujol, M. C.; Mateos, X.; Aznar, A.; Solans, X.; Suriñach, S.; Massons, J.; Díaz, F.; Aguiló, M. Structural Redetermination, Thermal Expansion and Refractive Indices of $KLu(WO_4)_2$. *J. Appl. Crystallogr.* **2006**, *39*, 230−236.
(96) Pujol, M. C.; Mateos, X.; Solé, R.; Massons, J.; Gavaldà, J.; Solans, X.; Díaz, F.; Aguiló, M. Structure, Crystal Growth and Physical Anisotropy of $KYb(WO_4)_2$, a New Laser Matrix. *J. Appl. Crystallogr.* **2002**, *35*, 108−112.
(97) Borowiec, M. T.; Dyakonov, V. P.; Woźniak, K.; Dobrzycki, Ł.; Berkowski, M.; Zubov, E. E.; Michalski, E.; Szewczyk, A.; Gutowska, M. U.; Zayarnyuk, T.; Szymczak, H. Crystal Structure and Magnetic Properties of Potassium Erbium Double Tungstate $KEr(WO_4)_2$. *J. Phys.: Condens. Matter* **2007**, *19*, 056206.
(98) Gallucci, E.; Goutaudier, C.; Boulon, G.; Cohen-Adad, M. T.; Mentzen, B. F. Nonstoichiometric $KY(WO_4)_2$: Crystal Growth, Chemical and Physical Characterization. *J. Cryst. Growth* **2000**, *209*, 895−905.
(99) Borowiec, M. T.; Dyakonov, V. P.; Wozniak, K.; Dobrzycki, L.; Majchrowski, A.; Michalski, E.; Zubov, E. E.; Khatsko, E. N.; Zayarnyuk, T.; Szewczyk, A.; et al. Crystalline Structure of Potassium Holmium Double Tungstate. *Acta Phys. Polym., A* **2011**, *119* (6), 835−837.
(100) Gateshki, M.; Igartua, J. M. Second-Order Structural Phase Transition in Sr_2CuWO_6 Double-Perovskite Oxide. *J. Phys.: Condens. Matter* **2003**, *15*, 6749−6757.
(101) Alvarez-Vega, M.; Rodriguez-Carvajal, J.; Reyes-Cardenas, J. G.; Fuentes, A. F.; Amador, U. Synthesis and Characterization of New Double Tungstates $Li_2M^{II}(WO_4)_2$ (M = Co, Ni, and Cu). *Chem. Mater.* **2001**, *13*, 3871−3875.
(102) McDowell, N. A.; Knight, K. S.; Lightfoot, P. Unusual High-Temperature Structural Behaviour in Ferroelectric Bi_2WO_6. *Chem. - Eur. J.* **2006**, *12*, 1493−1499.
(103) Shen, R.; Wang, C.; Wang, T. M.; Dong, C.; Chen, X. L.; Liang, J. K. Crystal Structures of $Dy_2(WO_4)_3$ and $GdY(WO_4)_3$. *Rare Met.* **2003**, *22* (1), 49−54.
(104) Templeton, D. H.; Zalkin, A. Crystal Structure of Europium Tungstate. *Acta Crystallogr.* **1963**, *16*, 762−766.
(105) Polyanskaya, T. M.; Borisov, S. V.; Belov, N. V. The Crystal Structure of $Pr_3WO_6Cl_3$. *Dokl. Akad. Nauk SSSR* **1969**, *187*, 1043−1046.
(106) Parise, J. B.; Brixner, L. H.; Prince, E. Refinement of the Structure of Trilanthanum Trichlorohexaoxotungstate, $La_3WO_6Cl_3$, from Neutron Powder Diffraction Data. *Acta Crystallogr., Sect. C: Cryst. Struct. Commun.* **1983**, *39*, 1326−1328.
(107) Michel, C.; Guyomarc'h, A.; Raveau, B. Nouveaux Echangeurs Cationiques Avec Une Structure a Tunnels Entrecroises: Les Oxydes $A_{12}M_{33}O_{90}$ et $A1_2M_{33}O_{90}$, 12 H_2O. *J. Solid State Chem.* **1977**, *22*, 393−403.
(108) Kim, J. S.; Lee, J. C.; Cheon, C. I.; Kang, H. J. Crystal Structures and Low Temperature Cofiring Ceramic Property of (1-x)(Li, RE)W_2O_8-x$BaWO_4$ Ceramics (RE = Y, Yb). *Japanese J. Appl. Physics, Part 1 Regul. Pap. Short Notes Rev. Pap* **2006**, *45*, 7397−7400.
(109) Kondo, R. The Synthesis and Crystallography of a Group of New Compounds Belonging to the Hauyne Type Structure. *Yogyo Kyokaishi* **1965**, *73*, 101−108.
(110) Müller-Buschbaum, H.; Sedello, O. Die Kristallstrukturen von A-$CuGdW_2O_8$ Und $CuNdMo_2O_8$. *J. Alloys Compd.* **1994**, *204*, 237−241.
(111) Klevtsova, R. F.; Kharchenko, L. Y.; Borisov, S. V.; Efremov, V. A.; Klevtsov, P. V. Triclinic Modification of Lithium-Rare Earth Tungstates Li Ln (W $O_4)_2$, Where Ln Is La-Sm. *Kristallografiya* **1979**, *24*, 446−454.
(112) Gressling, T.; Müller-Buschbaum, H. Ein Neuer Strukturtyp Bei Kupfer-Lanthanoid-Oxowolframaten: $CuDy_5(WO_4)_8$. *Z. Anorg. Allg. Chem.* **1995**, *621*, 181−185.
(113) Shigematsu, H.; Nomura, K.; Nishiyama, K.; Tojo, T.; Kawaji, H.; Atake, T.; Kawamura, Y.; Miyoshi, T.; Matsushita, Y.; Tanaka, M.; et al. Structures and Phase Transitions in Rb_2MoO_4 and Rb_2WO_4. *Ferroelectrics* **2011**, *414*, 195−200.
(114) Chang, H. Y.; Sivakumar, T.; Ok, K. M.; Halasyamani, P. S. Polar Hexagonal Tungsten Bronze-Type Oxides: $KNbW_2O_9$, $RbNbW_2O_9$, and $KTaW_2O_9$. *Inorg. Chem.* **2008**, *47*, 8511−8517.
(115) Rozanova, O. N.; Pol'shchikova, Z. Y.; Kovba, L. M. Crystal Structure of Uranium Tungstate U (W $O_4)_2$. *Radiokhimiya* **1978**, *20*, 125−127.
(116) Singh, D. J. Relationship of Li_2WO_4 to the Scheelite Tungstate Scintillators: Electronic Structure and Atomic Positions from Density-Functional Calculations. *Phys. Rev. B: Condens. Matter Mater. Phys.* **2008**, *77*, 113101.
(117) Zachariasen, W. H.; Plettinger, H. A. The Crystal Structure of Lithium Tungstate. *Acta Crystallogr.* **1961**, *14*, 229−230.
(118) Abrahams, S. C.; Bernstein, J. L. Crystal Structure of the Transition-Metal Molybdates and Tungstates. II. Diamagnetic $Sc_2(WO_4)_3$. *J. Chem. Phys.* **1966**, *45*, 2745−2752.
(119) Richard, A. P.; Edwards, D. D. Subsolidus Phase Relations and Crystal Structures of the Mixed-Oxide Phases in the In_2O_3-WO_3 System. *J. Solid State Chem.* **2004**, *177*, 2740−2748.
(120) Lamire, M.; Labbé, P.; Goreaud, M.; Raveau, B. $Ba_2P_8W_{32}O_{112}$: Structural Study in Comparison with the K and Rb Diphosphate Tungsten Bronzes with Hexagonal Tunnels. *J. Solid State Chem.* **1987**, *71*, 342−348.
(121) Chakraborty, K. R.; Das, A.; Krishna, P. S. R.; Yusuf, S. M.; Patwe, S. J.; Achary, S. N.; Tyagi, A. K. A Low Temperature Magnetization and Neutron Diffraction Study of Ca_2NiWO_6. *J. Alloys Compd.* **2008**, *457*, 15−18.
(122) Horiuchi, H.; Morimoto, N.; Yamaoka, S. The Crystal Structure of Li_2WO_4 II: A Structure Related to Spinel. *J. Solid State Chem.* **1979**, *30*, 129−135.
(123) Depmeier, W.; Yamamoto, A. Powder Profile Refinement of a Commensurately Modulated Aluminate Sodalite. *Mater. Sci. Forum* **1991**, *79*−*82*, 763−768.
(124) Champarnaud-Mesjard, J.-C.; Frit, B.; Watanabe, A. Crystal Structure of $Bi_2W_2O_9$, the n=2 Member of the Homologous Series $(Bi_2O_2)B^{VI}{}_nO_{3n+1}$ of Cation-Deficient Aurivillius Phases. *J. Mater. Chem.* **1999**, *9*, 1319−1322.
(125) Jorgensen, J.; Hu, Z.; Teslic, S.; Argyriou, D.; Short, S.; Evans, J.; Sleight, A. Pressure-Induced Cubic-to-Orthorhombic Phase Transition in ZrW_2O_8. *Phys. Rev. B: Condens. Matter Mater. Phys.* **1999**, *59*, 215−225.
(126) Okada, K.; Ossaka, J. Caesium Lithium Tungstate: A Stuffed H-Cristobalite Structure. *Acta Crystallogr., Sect. B: Struct. Crystallogr. Cryst. Chem.* **1980**, *36*, 657−659.
(127) Wang, K.; Zhang, J.; Wang, J.; Yu, W.; Zhang, H.; Wang, X.; Wang, Z.; Ba, M. Growth, Structure and Morphology Study of Monoclinic $RbGd(WO_4)_2$ Crystals. *J. Cryst. Growth* **2005**, *281*, 407−410.
(128) Xie, H.; Shen, D.; Xie, C.; Wang, X.; Shen, G. Crystal Growth and Structure of $KBi(WO_4)_2$ Single Crystals. *Cryst. Res. Technol.* **2006**, *41*, 961−966.
(129) Borowiec, M. T.; Prokhorov, A. D.; Krygin, I. M.; Dyakonov, V. P.; Woźniak, K.; Dobrzycki; Zayarnyuk, T.; Barański, M.; Domuchowski, W.; Szymczak, H. Crystal Structure and EPR of the $RbNd(WO_4)_2$ Single Crystal. *Phys. B* **2006**, *371*, 205−209.
(130) Obbade, S.; Dion, C.; Bekaert, E.; Yagoubi, S.; Saadi, M.; Abraham, F. Synthesis and Crystal Structure of New Uranyl Tungstates $M_2(UO_2)(W_2O_8)$ (M=Na, K), $M_2(UO_2)_2(WO_5)O$ (M=K, Rb), and $Na_{10}(UO_2)_8(W_5O_{20})O_8$. *J. Solid State Chem.* **2003**, *172*, 305−318.
(131) Obbade, S.; Yagoubi, S.; Dion, C.; Saadi, M.; Abraham, F. Two New Lithium Uranyl Tungstates $Li_2(UO_2)(WO_4)_2$ and $Li_2(UO_2)_4(WO_4)_4O$ with Framework Based on the Uranophane Sheet Anion Topology. *J. Solid State Chem.* **2004**, *177*, 1681−1694.
(132) Horiuchi, H.; Morimoto, N.; Yamaoka, S. The Crystal Structure of Li_2WO_4 (IV) and Its Relation to the Wolframite-Type Structure. *J. Solid State Chem.* **1980**, *33*, 115−119.
(133) Huang, J.; Xu, J.; Li, H.; Luo, H.; Yu, X.; Li, Y. Determining the Structure of Tetragonal Y_2WO_6 and the Site Occupation of Eu^3 Dopant. *J. Solid State Chem.* **2011**, *184* (4), 843−847.

DOI: 10.1021/acssuschemeng.5b00369
ACS Sustainable Chem. Eng. 2015, 3, 2112−2129

(134) Stomberg, R. Structure of Potassium tetraperoxotungstate(VI), $K_2[W(O_2)_4]$. *J. Less-Common Met.* **1988**, *143*, 363−371.
(135) Depmeier, W. Structure of Cubic Aluminate Sodalite $Ca_8[Al_{12}O_{24}](WO_4)_2$ in Comparison with Its Orthorhombic Phase and with Cubic $Sr_8[Al_{12}O_{24}](CrO_4)_2$. *Acta Crystallogr., Sect. B: Struct. Sci.* **1988**, *44*, 201−207.
(136) Knight, K. S. The Crystal Structure of Russellite; a Re-Determination Using Neutron Powder Diffraction of Synthetic Bi_2WO_6. *Mineral. Mag.* **1992**, *56*, 399−409.
(137) Gärtner, M.; Abeln, D.; Pring, A.; Wilde, M.; Reller, A. Synthesis, Structure, and Reactivity of Novel Lanthanum Tungstates. *J. Solid State Chem.* **1994**, *111*, 128−133.
(138) Jeannin, Y.; Launay, J. P.; Sedjadi, M. A. S. Crystal and Molecular Structure of the Six-Electron-Reduced Form of Metatungstate $Rb_4H_8[H_2W_{12}O_{40}](H_2O)_{18}$: Occurrence of a Metal-Metal Bonded Subcluster in a Heteropolyanion Framework. *Inorg. Chem.* **1980**, *19*, 2933−2935.
(139) Fourquet, J. L.; Le Bail, A.; Gillet, P. A. $LiNbWO_6$: Crystal Structure of Its Two Allotropic Forms. *Mater. Res. Bull.* **1988**, *23*, 1163−1170.
(140) Knyazev, A. V.; Maczka, M.; Kuznetsova, N. Y. Thermodynamic Modeling, Structural and Spectroscopic Studies of the $KNbWO_6$-$KSbWO_6$-$KTaWO_6$ System. *Thermochim. Acta* **2010**, *506*, 20−27.
(141) Knyazev, A. V.; Kuznetsova, N. Y. Crystal Structure of Compounds $CsA^{V}A'^{VI}O_6$ (A^{V} = Sb, Ta; A'^{VI} = W, U). *Radiochemistry* **2009**, *51*, 1−4.
(142) Murphy, D.; Cava, R.; Rhyne, K.; Roth, R.; Santoro, A.; Zahurak, S.; Dye, J. Structural Aspects of Insertion Reactions of the Pyrochlore, $KNbWO_6$. *Solid State Ionics* **1986**, *18−19*, 799−801.
(143) Pakhomov, V. I.; Fedorov, P. M.; Okunera, A. S.; Sorokina, O. V. Structure and Elastic Properties of $AgIn(WO_4)_2$. *Koord. Khimiya* **1977**, *3*, 765−767.
(144) Postema, J. M.; Fu, W. T.; Ijdo, D. J. W. Crystal Structure of $LiLnW_2O_8$ (Ln=lanthanides and Y): An X-Ray Powder Diffraction Study. *J. Solid State Chem.* **2011**, *184* (8), 2004−2008.
(145) Tyagi, M.; Singh, S. G.; Sangeeta; Prasad, R.; Auluck, S.; Singh, D. J. A Study of Electronic and Optical Properties of $NaBi(WO_4)_2$: A Disordered Double Tungstate Crystal. *Phys. B* **2010**, *405*, 3267−3271.
(146) Bonin, M.; Paciorek, W.; Schenk, K. J.; Chapuis, G. X-Ray Study of and Structural Approach to the Incommensurate Perovskite Pb_2CoWO_6. *Acta Crystallogr., Sect. B: Struct. Sci.* **1995**, *51*, 48−54.
(147) Zhengmin, F.; Wenxiu, L. Crystal Structure of the High-Temperature Phase of a Compound Sr_2ZnWO_6. *Powder Diffr.* **1992**, *7*, 226−227.
(148) Patwe, S. J.; Achary, S. N.; Mathews, M. D.; Tyagi, A. K. Synthesis, Phase Transition and Thermal Expansion Studies on M_2MgWO_6 (M = Ba^{2+} and Sr^{2+}) Double Perovskites. *J. Alloys Compd.* **2005**, *390*, 100−105.
(149) Martínez-Lope, M. J.; Alonso, J. A.; Casais, M. T.; Fernández-Díaz, M. T. Preparation, Crystal and Magnetic Structure of the Double Perovskites Ba_2CoBO_6 (B = Mo, W). *Eur. J. Inorg. Chem.* **2002**, *2002*, 2463−2469.
(150) Cox, D. E.; Shirane, G.; Frazer, B. C. Neutron-Diffraction Study of Antiferromagnetic Ba_2CoWO_6 and Ba_2NiWo_6. *J. Appl. Phys.* **1967**, *38*, 1459−1460.
(151) Azad, A. K.; Eriksson, S.-G.; Mellergård, A.; Ivanov, S. A.; Eriksen, J.; Rundlöf, H. A Study on the Nuclear and Magnetic Structure of the Double Perovskites A_2FeWO_6 (A = Sr, Ba) by Neutron Powder Diffraction and Reverse Monte Carlo Modeling. *Mater. Res. Bull.* **2002**, *37*, 1797−1813.
(152) Baldinozzi, G.; Sciau, P.; Buffat, P.-A. Investigation of the Orthorhombic Structures of Pb_2MgWO_6 and Pb_2CoWO_6. *Solid State Commun.* **1993**, *86* (9), 541−544.
(153) Bugaris, D. E.; Hodges, J. P.; Huq, A.; zur Loye, H.-C. Crystal Growth, Structures, and Optical Properties of the Cubic Double Perovskites Ba_2MgWO_6 and Ba_2ZnWO_6. *J. Solid State Chem.* **2011**, *184* (8), 2293−2298.
(154) Fu, W. T.; Akerboom, S.; IJdo, D. J. W. Crystal Structures of the Double Perovskites $Ba_2Sr_{1-x}Ca_xWO_6$. *J. Solid State Chem.* **2007**, *180* (5), 1547−1552.
(155) Klevtsov, P. V.; Klevtsova, R. F. Single-Crystal Synthesis and Investigation of the Double Tungstates $NaR^{3+}(WO_4)_2$, Where R^{3+} = Fe, Sc, Ga, and In. *J. Solid State Chem.* **1970**, *2*, 278−282.
(156) Keeling, R. O. The Structure of $NiWO_4$. *Acta Crystallogr.* **1957**, *10*, 209−213.
(157) Shimony, Y.; Ben-Dor, L. On the Crystal Structure of $CrWO_4$. *Mater. Res. Bull.* **1983**, *18*, 331−335.
(158) Errandonea, D.; Pellicer-Porres, J.; Manjón, F. J.; Segura, A.; Ferrer-Roca, C.; Kumar, R. S.; Tschauner, O.; Rodríguez-Hernández, P.; López-Solano, J.; Radescu, S.; et al. High-Pressure Structural Study of the Scheelite Tungstates $CaWO_4$ and $SrWO_4$. *Phys. Rev. B: Condens. Matter Mater. Phys.* **2005**, *72*, 174106.
(159) Velikodnyi, Y. A.; Trunov, V. K. Structure of the Double Wolframate $NaIn(WO_4)_2$. *Zhurnal Strukt. Khimii* **1971**, *12*, 334.
(160) Errandonea, D.; Pellicer-Porres, J.; Manjón, F. J.; Segura, A.; Ferrer-Roca, C.; Kumar, R. S.; Tschauner, O.; López-Solano, J.; Rodríguez-Hernández, P.; Radescu, S.; et al. Determination of the High-Pressure Crystal Structure of $BaWO_4$ and $PbWO_4$. *Phys. Rev. B: Condens. Matter Mater. Phys.* **2006**, *73*, 224103.
(161) Baldinozzi, G.; Sciau, P.; Lapasset, J. Crystal Structure of Pb_2CoWO_6 in the Cubic Phase. *Phys. Status Solidi* **1992**, *133*, 17−23.
(162) Becka, L. N.; Poljak, R. Estructura Cristalina Del MoO_4Na_2 Y Del WO_4Na_2. *An. la Asoc. Quim. Argentina* **1958**, *46*, 204−209.
(163) Cheviré, F.; Tessier, F.; Marchand, R. New Scheelite-Type Oxynitrides in Systems RWO_3N-AWO_4 (R = Rare-Earth Element; A = Ca, Sr) from Precursors Obtained by the Citrate Route. *Mater. Res. Bull.* **2004**, *39*, 1091−1101.
(164) Zhao, D.; Li, F.; Cheng, W.; Zhang, H. Scheelite-Type $NaDy(WO_4)_2$. *Acta Crystallogr., Sect. E: Struct. Rep. Online* **2010**, *66*, i2.
(165) Hanuza, J.; Benzar, A.; Haznar, A.; Maczka, M.; Pietraszko, A.; Van Der Maas, J. H. Structure and Vibrational Dynamics of Tetragonal $NaBi(WO_4)_2$ Scheelite Crystal. *Vib. Spectrosc.* **1996**, *12*, 25−36.
(166) Li, H.; Hong, G.; Yue, S. Crystal Study of $NaLn(WO_4)_2$ (Ln= La, Pr, Nd). *Zhongguo Xitu Xuebao* **1990**, *8*, 37−41.
(167) Perets, S.; Tseitlin, M.; Shneck, R. Z.; Mogilyanski, D.; Kimmel, G.; Burshtein, Z. Sodium Gadolinium Tungstate $NaGd(WO_4)_2$: Growth, Crystallography, and Some Physical Properties. *J. Cryst. Growth* **2007**, *305*, 257−264.
(168) Xu, K.-Q.; Xue, J.-Y.; Ding, Y.; Lu, G.-G. Discovery of Stolzite in China and Refinement of Its Crystal Structure. *Dizhi Xuebao* **1994**, *68*, 287−292.
(169) De Moraes, J. R.; Baldochi, S. L.; Soares, L.; dos, R. L.; Mazzocchi, V. L.; Parente, C. B. R.; Courrol, L. C. Growth, Structural and Optical Characterizations of $LiLa_{(1-x)}Eu_x(WO_4)_2$ Single-Crystalline Fibers by the Micro-Pulling-down Method. *Mater. Res. Bull.* **2012**, *47*, 744−749.
(170) Klevtsova, R. F.; Bakakin, V. V.; Solodovnikov, S. F.; Glinskaya, L. A. The Combination of the Wolframite's and Scheelite's Motives in the Crystal Structure of Sodium and Zirconium Tungstate $Na_2ZrW_3O_{12}$ = $Na_2ZrW_2O_8(WO_4)$. *Zhurnal Strukt. Khimii* **1981**, *22*, 6−11.
(171) Gokhman, L. Z.; Dzhurinskii, B. F.; Efremov, V. A.; Ilyukhin, A. B.; Chistova, V. I. Synthesis and Structure of Boratotungstates Ln_3BWO_9 (Ln = La, Pr, Nd, Sm-Ho). *Zh. Neorg. Khim.* **1994**, *39*, 1075−1079.
(172) Han, X.; Lin, Z.; Hu, Z.; Wang, G. Structure of $KLa(WO_4)_2$ with a Novel Isolated La Polyhedron. *Mater. Res. Innovations* **2002**, *6*, 118−121.
(173) Torardi, C. C.; Page, C.; Brixner, L. H.; Blasse, G.; Dirksen, G. J. Structure and Luminescence of Some $CsLnW_2O_8$ Compounds. *J. Solid State Chem.* **1987**, *69*, 171−178.
(174) Ra, H. S.; Ok, K. M.; Halasyamani, P. S. Combining Second-Order Jahn-Teller Distorted Cations to Create Highly Efficient SHG Materials: Synthesis, Characterization, and NLO Properties of $BaTeM_2O_9$ (M = Mo^{6+} or W^{6+}). *J. Am. Chem. Soc.* **2003**, *125*, 7764−7765.

DOI: 10.1021/acssuschemeng.5b00369
ACS Sustainable Chem. Eng. 2015, 3, 2112−2129

(175) Mączka, M.; Tomaszewski, P.; Stępień-Damm, J.; Majchrowski, A.; Macalik, L.; Hanuza, J. Crystal Structure and Vibrational Properties of Nonlinear Eu_3BWO_9 and Nd_3BWO_9 Crystals. *J. Solid State Chem.* **2004**, *177*, 3595−3602.
(176) Goodey, J.; Ok, K. M.; Broussard, J.; Hofmann, C.; Escobedo, F. V.; Halasyamani, P. S. Syntheses, Structures, and Second-Harmonic Generating Properties in New Quaternary Tellurites: $A_2TeW_3O_{12}$ (A=K, Rb, or Cs). *J. Solid State Chem.* **2003**, *175*, 3−12.
(177) Range, K.-J.; Klement, U.; Rau, F.; Schiessl, U.; Heyns, A. M. Crystal Structure of Rubidium ditungstate(VI), $Rb_2W_2O_7$. *Z. Kristallogr.* **1993**, *203*, 318−319.
(178) Moutou, J. M.; Vlasse, M.; Cervera-Marzal, M.; Chaminade, J. P.; Pouchard, M. A Structural Study of a New Lithium Oxyfluorotungstate, LiW_3O_9F. *J. Solid State Chem.* **1984**, *51*, 190−195.
(179) Hong, H.-P.; Dwight, K. Crystal Structure and Fluorescence Lifetime of a Laser Material $NdNa_5(WO_4)_4$. *Mater. Res. Bull.* **1974**, *9*, 775−780.
(180) Klevtsova, R. F.; Volkova, L. M. Crystal Structure of Monoclinic $KNd(WO_4)_2$. *Kristallografiya* **1972**, *17*, 859−861.
(181) Zikmund, Z. The Crystal Structure of $Ca_3WO_6Cl_2$ and the Configuration of the WO_5^{4-} Ion. *Acta Crystallogr., Sect. B: Struct. Crystallogr. Cryst. Chem.* **1974**, *30*, 2587−2593.
(182) Klevtsova, R. F.; Borisov, S. V. The Crystal Structure of $NdWO_4(OH)$. *Kristallografiya* **1969**, *14*, 904−907.
(183) Li, J.; Pan, S.; Zhao, W.; Tian, X.; Han, J.; Fan, X. Synthesis and Crystal Structure of a Novel Boratotungstate: $Pb_6B_2WO_{12}$. *Solid State Sci.* **2011**, *13*, 966−969.
(184) Brudgam, I.; Fuchs, J.; Hartl, H.; Palm, R. Two New isopolyoxotungstates(VI) with the Empirical Composition $Cs_2W_2O_7$ * $2(H_2O)$ and $Na_2W_2O_7$ * H_2O: A Icosatetratungstate and a Polymeric Compound. *Angew. Chem., Int. Ed.* **1998**, *37*, 2668−2671.
(185) Meredig, B.; Wolverton, C. A Hybrid Computational-Experimental Approach for Automated Crystal Structure Solution. *Nat. Mater.* **2013**, *12*, 123−127.
(186) Yang, L.; Dacek, S.; Ceder, G. Proposed Definition of Crystal Substructure and Substructural Similarity. *Phys. Rev. B: Condens. Matter Mater. Phys.* **2014**, *90* (5), 1−9.
(187) Fuchs, A. H.; Cheetham, A. K. Adsorption of Guest Molecules in Zeolitic Materials: Computational Aspects. *J. Phys. Chem. B* **2001**, *105* (31), 7375−7383.
(188) Akten, E. D.; Siriwardane, R.; Sholl, D. S. Monte Carlo Simulation of Single- and Binary-Component Adsorption of CO_2, N_2, and H_2 in Zeolite Na-4A. *Energy Fuels* **2003**, *17* (7), 977−983.
(189) Corma, A.; Garcia, H. Supramolecular Host-Guest Systems in Zeolites Prepared by Ship-in-a-Bottle Synthesis. *Eur. J. Inorg. Chem.* **2004**, *2004*, 1143−1164.
(190) Ravoo, B. J. Nanofabrication with Metal Containing Dendrimers. *Dalton Trans.* **2008**, No. 12, 1533−1537.

DOI: 10.1021/acssuschemeng.5b00369
ACS Sustainable Chem. Eng. 2015, 3, 2112−2129